AD-A143 773 IGNITION AND FLAME PROPAGATION IN SPRAYS(U) 1/1
CARNEGIE-MELLON UNIV PITTSBURGH PA DEPT OF MECHANICAL
ENGINEERING S K AGGARWAL ET AL. 10 JUL 84
UNCLASSIFIED ARO-17001.7-EG DAAG29-80-C-0002 F/G 21/2 NL

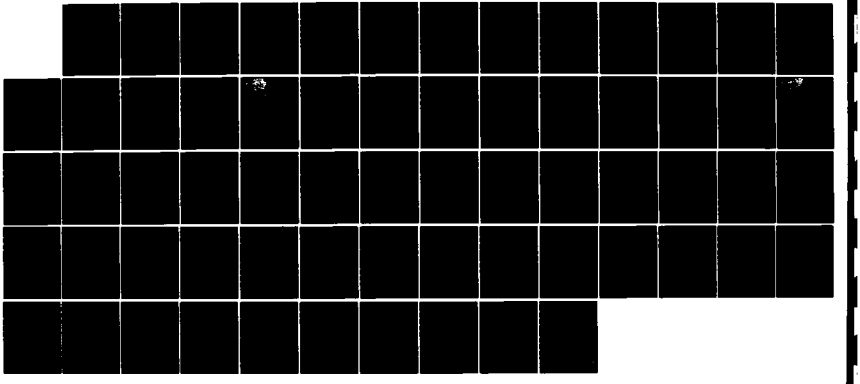

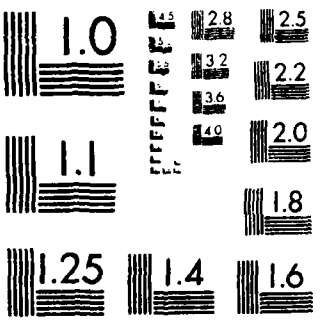

AD-A143 773

UNCLASSIFIED
SECURITY CLASSIFICATION OF THIS PAGE (When Data Entered)

REPORT DOCUMENTATION PAGE	READ INSTRUCTIONS BEFORE COMPLETING FORM
1. REPORT NUMBER: ARO 17001.7-EG	2. GOVT ACCESSION NO.: N/A AD-A143773
	3. RECIPIENT'S CATALOG NUMBER: N/A
4. TITLE (and Subtitle): IGNITION AND FLAME PROPAGATION IN SPRAYS	5. TYPE OF REPORT & PERIOD COVERED: FINAL REPORT 1 Dec 79 - 31 Jan 84
	6. PERFORMING ORG. REPORT NUMBER
7. AUTHOR(s): AGGARWAL, S.K., ASHGRIZZADEH, N., SIRIGNANO, W.A., YAO, S.C.	8. CONTRACT OR GRANT NUMBER(s): DAAG 29-80-C-0002
9. PERFORMING ORGANIZATION NAME AND ADDRESS: Dept. of Mechanical Eng. Carnegie-Mellon University, Pittsburgh, PA 15213	10. PROGRAM ELEMENT, PROJECT, TASK AREA & WORK UNIT NUMBERS
11. CONTROLLING OFFICE NAME AND ADDRESS: U. S. Army Research Office Post Office Box 12211 Research Triangle Park, NC 27709	12. REPORT DATE: 7/10/84
	13. NUMBER OF PAGES
14. MONITORING AGENCY NAME & ADDRESS (if different from Controlling Office)	15. SECURITY CLASS. (of this report): Unclassified
	15a. DECLASSIFICATION/DOWNGRADING SCHEDULE

16. DISTRIBUTION STATEMENT (of this Report)

Approved for public release; distribution unlimited.

17. DISTRIBUTION STATEMENT (of the abstract entered in Block 20, if different from Report)

NA

18. SUPPLEMENTARY NOTES

The view, opinions, and/or findings contained in this report are those of the author(s) and should not be construed as an official Department of the Army position, policy, or decision, unless so designated by other documentation.

19. KEY WORDS (Continue on reverse side if necessary and identify by block number)

SPRAY COMBUSTION, IGNITION, FLAME, MODELING

20. ABSTRACT (Continue on reverse side if necessary and identify by block number)

An experimental and numerical analysis of ignition and flame propagation in sprays is done. A unique multi-orifice impulsed spray generator is designed and developed. This spray generator is capable of producing arrays of droplets, with controllable droplet size and spacings.

Radiation effect on the droplet evaporation in spray, upstream of the flame front is studied through analytical modeling.

(continued on back)

DD FORM 1 JAN 73 1473 EDITION OF 1 NOV 65 IS OBSOLETE

UNCLASSIFIED
SECURITY CLASSIFICATION OF THIS PAGE (When Data Entered)

An extensive numerical optimization study has been performed to compare the efficiency of several explicit and implicit schemes, and a numerical code has been developed to study a stabilized laminar flame in two-phase mixtures. A hybrid Eulerian-Lagrangian scheme has been developed to solve the gas and liquid phase equations.

Both experimental and numerical parametric study of controlled sprays combustion is completed and effects of droplet size, fuel type, chemical kinetics, equivalence ratio and droplet heating models have been examined.

Through these studies two different flame propagation mechanisms are revealed. Depending on fuel vapor/air mixture ratio at the flame front, the flame propagation mechanism, can be kinetically controlled or diffusion controlled.

IGNITION AND FLAME PROPAGATION IN SPRAYS

FINAL REPORT

S.K. AGGARWAL
N. ASHGRIZZADEH
W.A. SIRIGNANO
S.C. YAO

DATE: 10 July, 1984

U.S. ARMY RESEARCH OFFICE

Contract #DAAG29-80-C-0002

CARNEGIE-MELLON UNIVERSITY

TABLE OF CONTENTS

LIST OF APPENDIXES

INTRODUCTION

Combustion of the liquid fuels, through atomization and vaporization, will remain the primary mode of fossil fuel energy conversion for the next several decades. It finds a wide range of applications such as in variety of gas turbine engines, diesel and fuel-injected spark engines, industrial boilers and liquid rocket motors. The spray combustion in all these systems is a complex phenomena involving: (i) atomization of liquid fuels, which produces droplets of different sizes and velocities (ii) mixing of the droplets with oxidant and hot combustion products (iii) vaporization of the droplets (iv) mixing of the fuel vapor with surrounding gas by diffusion and convection processes and (v) chemical reaction. The tasks of improving combustion efficiency and pollutant levels require a fundamental understanding of these physical and chemical processes. Because of the complexity of the problem, a simultaneous enhancement is needed in experimental measurements and predictive capabilities of spray combustion phenomena. With this objective in mind, an ARO-sponsored theoretical-experimental program has been underway at Carnegie-Mellon University for the past four years.

THEORETICAL EFFORT

This section summarizes the theoretical and numerical efforts in enhancing the fundamental understanding of spray combustion processes. This research has been supported by Army Research Office and covers a four-year period from 1979 to 1983. During this period, several major tasks have been completed. These include:

1. the study of enclosed, unsteady one-dimensional laminar and turbulent flame propagation in homogeneous and heterogeneous mixtures,
2. the efficiency comparison of several explicit and implicit finite-difference schemes for solving laminar homogeneous and heterogeneous enclosed deflagrations,
3. the efficiency and accuracy comparison of explicit, implicit and operator-splitting techniques for axisymmetric spray vaporization problem,
4. the study of one-dimensional steady laminar flame propagation in one-phase and two-phase mixtures,
5. the development of hybrid (Eulerian-Lagrangian) numerical code for one-dimensional, reacting air-fuel droplet-fuel vapor flows,
6. computation of spray flame speeds and a preliminary comparison with experimental results,
7. a parametric study to examine the effects of droplet size, equivalence ratio, fuel type, droplet heating models, chemical kinetics, and grid size and
8. the examination of different gas and liquid phase models which are used in spray vaporization and combustion processes.

Task 1 is discussed in a paper (see addenda) presented at the 1980 ASME Winter Annual Meeting. In this study, the gas turbulence was modeled through a two-equation (k-ϵ) model and the particle turbulence was neglected. The major conclusion was that the characteristics of turbulent flame propagation in both homogeneous and heterogeneous mixtures depend on a turbulence delay time defined by the parameter k/ϵ, and turbulence generation time which is related to the chemical reaction time. Task 2 evaluated the effectiveness of several explicit and implicit finite-difference methods for computing the unsteady laminar flames in homogeneous as well as heterogeneous mixtures. The details are given in Refs. 2 and 3 (see

addenda). A similar study has been performed under Task 3, where vaporizing spray is considered in a gaseous jet flow. The effectiveness curves are obtained for four different finite-difference schemes. The results are detailed in the paper submitted for publication in Journal of Computational Physics (Ref. 4).

These are two major objectives for Tasks 4-6. The first is to develop an efficient numerical code to model the two-phase processes which occur in laminar spray flames. The results of this code are expected to provide global as well as detailed local information about the spray flame phenomena. The global information may include the flame speed, the influence of various parameters on the flame speed, and the identification of dominant burning mechanism of the spray flame. The second objective is to provide numerical results for making comparison with the results of the parallel experimental study. A hybrid Eulerian-Lagrangian code has been developed, the laminar spray flame speeds have been computed, a limited parametric study has been conducted, and some preliminary comparison has been made with the experiments. These efforts are detailed in Ref. 5-7. At present the numerical code is being modified to include the polydispersed spray, more sophisticated droplet-heating models and the multicomponent fuel droplets. The probabilistic character of the spray and the droplet group combustion behavior will also be included in a later study.

Under Task 7, the hybrid numerical code has been employed to perform a detailed parametric study of flame propagation in confined sprays. Some results are given in Ref. 8. Additional results will are presented in Ref. 9. Under Task 9, capabilities have been developed to include more sophisticated gas-phase and liquid-phase models for representing the inter-phase processes. A comparison of various models for an isolated droplet and for a vaporizing spray is given in Ref. 10.

EXPERIMENTAL EFFORT

An experimental study of ignition and flame propagation in sprays is achieved by studying evaporation and combustion of a well controlled spray. During this research a unique spray generator is designed and developed which is capable of producing a well controlled droplet flow. Later this spray is burned and effect of important parameters such as droplet diameter, air/fuel rates, and fuel type on the combustion phenomena is studied. Also, an analytical study of the radiative evaporation of the fuel droplet flow at the upstream of the flame is done. In following sections a brief discussion of each of above work, with reference to corresponding publications are given.

SPRAY GENERATOR

In order to generate a well controlled droplet flow spray, a multi-orifice impulsed spray generator with two different modes of operation is developed. The impulse jet operation mode covers a wide range of droplet frequencies, and produces arrays of droplets with controllable spacing, but with a wide size spectrum. This ejector also operates in pressurized flow mode. In this mode, optimum disturbance frequency breaks up the liquid jets into uniform size droplets, resulting in a monosized spray. Precise control of fuel flow rate and droplet size is obtained. The details of design and operation of multi-orifice impulsed spray generator is given in publications generated from this research listed in references 11-13. Reference 13 is included in the appendix.

SPRAY COMBUSTION STUDIES

In order to study the combustion behavior of the spray generated by the present device, a special experimental set up is fabricated (13). The experimental study of the monodispersed spray of various fuels identified three major combustion phenomena. The all-blue flame of premixed gas combustion; the isolated droplet burning and propagation; and the mixed feature of premixed gas combustion and droplet burning where droplet cluster combustion is in this category.

Specific parametric studies have revealed that a dominant factor which is affecting the spray combustion phenomena and mechanism is the vapor fuel to liquid fuel ratio at the flame front. The amount of vapor fuel is dependent upon the droplet vaporization process which is, in turn dependent upon order factors. The mechanism of the flame propagation in sprays is governed by two different phenomena. One is kinetically controlled phenomena, and the other is diffusion controlled one. If there is enough prevaporization, or there is enough fuel vapor in the fresh mixture so that the fuel vapor/air mixture ratio ahead of the ignition zone is flammable then flame propagation is governed by the premixed, laminar or turbulent gas flame propagation. But if there is not enough vaporization, then overall fuel vapor/air mixture would not be flammable, although, it is observed that flame propagates in such sprays also. This type of flame propagation is different than that of premixed gas combustion. In such conditions the spray is either very dilute that relay type flame propagation is observed, where flame of an ignited droplet increases in size due to oxygen retardation, and eventually ignites the adjacent droplets. And, if spray is very rich, the group combustion phenomena is observed, where its mechanism is yet to be understood better. Both of these phenomena are diffusion controlled.

In order to see the effect of fuel vapor fraction on the flame propagation mechanism, experiments are done with three different fuels, Hexane, Heptane, and Octane. A multi-orifice plate with 47 orifices with 150μm diameter were used to do the experiment. The average initial droplet size for all three cases was 320 μm and overall equivalence ratio was kept constant at 1.8. Applied frequency was 3400 Hz. Initial fuel temperature was varied to change the fuel vapor fraction in the spray. As the initial fuel temperature is increased, more fuel is vaporized. As a result the fuel vapor fraction at the ignition point increases as fuel initial temperature increases. Figure 1 shows a plot of flame speed vs. initial fuel temperature. It is seen that the flame speed increases as the fuel temperature and thus the fuel vapor

fraction increases. But the rate of this increase is dependent on type of fuel. As the fuel becomes less volatile the rate of increase of flame speed becomes less. The flame speed for volatile fuel of iso-hexane can go as low as 20 cm/sec and increase to 80 cm/sec for initial temperature of 43°C. The results of this work will be published in near future.

RADIATIVE HEATING OF THE DROPLETS

The heating and evaporation of the fuel droplet flow at the upstream of the flame front are analyzed considering the effect of thermal radiation from the hot zone of the combustion system. The radiative transport in a typical cylindrical combustion chamber is calculated considering the hot wall, the emitting and absorbing combustion products, and the absorption of the two phase droplet flow. Analytical solution is obtained. The heating and evaporation of a single droplet by thermal radiation in cold air has also been studied. The transfer number B is modified to include the effect of radiation. With the presence of radiation the change of the droplet size will not follow the simple d^2 rule. At the extreme case of quiescent environment the droplet surface temperature passes through a peak before the droplet evaporates completely. As an approximation the radiative flux at the upstream of the flame front may be considered as a constant, and the subsequent calculation will be easier. Following the methodology outlined in this work, complicated situations may be analyzed. Details of this work are given in publications generated under this grant which are listed in references (14-15) and are included in the appendix.

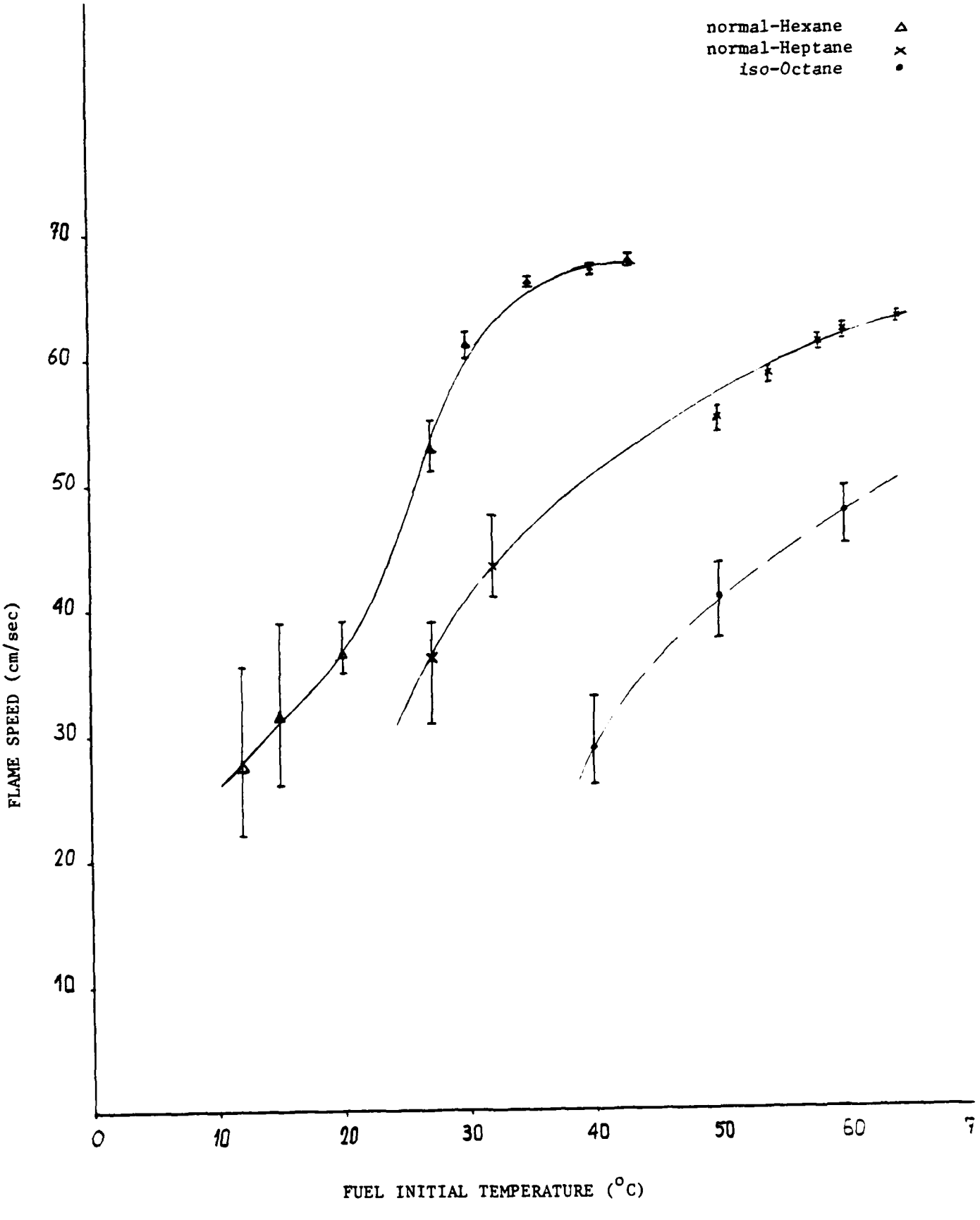
normal-Hexane
normal-Heptane
iso-Octane
70
60
50
40
30
20
10
0
10
20
30
40
50
60
FLAME SPEED (cm/sec)
FUEL INITIAL TEMPERATURE (°C)

LIST OF PARTICIPATING SCIENTIFIC PERSONNEL

1. Dr. S.K. AGGARWAL
2. ASHGRIZZADEH, N., EARNED Ph.D. DEGREE WHILE EMPLOYED ON THIS PROJECT
3. Professor N.A. SIRIGNANO
4. Professor S.C. YAO

REFERENCES

1. S.K. Aggarwal and W.A. Sirignano, "One-Dimensional Turbulent Flame Propagation in an Air-Fuel Droplet Mixture," ASME Winter Annual Meeting, Paper No. 80-WA/HT-37, 1980.

2. S.K. Aggarwal and W.A. Sirignano, "Effect of Numerical Modelling on One-Dimensional Enclosed Homogeneous and Heterogeneous Deflagrations," ASME Paper No. 81-WA/HT-46, 1981.

3. S.K. Aggarwal and W.A. Sirignano, "Numerical Modelling of One-Dimensional Homogeneous and Heterogeneous Deflagrations," to appear in *Computers and Fluids*, 1984.

4. S.K. Aggarwal, G. Fix, and W.A. Sirignano, "Two-Phase Axisymmetric Jet Flow: Explicit, Implicit and Split-Operation Calculations," submitted for publication in the *Journal of Compute. Phys.*.

5. S.K. Aggarwal and W.A. Sirignano, "A Study of One-Dimensional Steady Laminar Flame Propagation in Two-Phase Mixtures," Fall Technical Meeting, Eastern Section/Combustion Institute, Pittsburgh, PA, 1981.

6. S.K. Aggarwal and W.A. Sirignano, "A Computation of Laminar Spray Flames," Fall Technical Meeting, Eastern Section/Combustion Institute, Atlantic City, N.J., 1982.

7. S.K. Aggarwal, "Numerical Results on Steady Laminar Flames in Two-Phase Mixtures," Department Report, Department of Mechanical Engineering, Carnegie-Mellon University, Pittsburgh, August 1984.

8. S.K. Aggarwal, "A Hybrid Eulerian-Lagrangian Method for One-Dimensional Unsteady Spray Flames," Department Report, Department of Mechanical Engineering, Carnegie-Mellon University, Pittsburgh, July 1983.

9. S.K. Aggarwal and W.A. Sirignano, "Effect of Droplet Spacing on Spray Ignition and Flame Propagation Problem," to be submitted to *Combustion and Flame*.

10. S.K. Aggarwal, A.Y. Tong, and W.A. Sirignano, "A STudy of Inter-phase Exchange Laws in Spray Combustion Modelling," paper AIAA-83-0152, AIAA 21st Aerospace Meeting, Reno, Nevada, Jan. 10-13, 1980. Also submitted to AIAA Journal.

11. Ashgrizzadeh, N., and Yao, S.C., and Sirignano, W.A., "Progress on Impulse Jet Droplet Generator for Laminar Spray Combustion Experiments", Eastern Section/Combustion Institute, P.44, Princeton, N.J., 1980.

12. Ashgrizzadeh, N., and Yao. S.C., "Impulsed Spray Generator for Heterogeneous Combustion Experiments", Eastern Section/Combustion Institute, Atlantic City, N.J., 1982.

13. Ashgrizzadeh, N., and Yao, S.C., "Development of Multi-Orifice Impulsed Spray Generator for Heterogeneous Combustion Experiments", ASME/JSME

Thermal Engineering Joint Conference Proceeding, Volume Two, Paper No. 100158-B, Hawaii, 1983.

14. Yao, S.C. and Ashgrizzadeh, N., "Effect of Thermal Radiation on the Droplet Pre-evaporation in Spray Combustion", Eastern Section/Combustion Institute, P.39, Princeton, N.J., 1980.

15. Ashgrizzadeh, N. and Yao, S.C., "Radiative Effect on Droplet Pre-evaporation in Cylindrical Combustion Chambers", Eastern Section/Combustion Institute, P.129, Pittsburgh, PA. 1981.

80-WA/HT-37

THE AMERICAN SOCIETY OF MECHANICAL ENGINEERS
345 E 47 St., New York, N.Y. 10017

One-Dimensional Turbulent Flame Propagation in an Air-Fuel Droplet Mixture

S. K. Aggarwal

W. A. Sirignano

Carnegie-Mellon University,
Department of Mechanical Engineering,
Pittsburgh, Pa.

The turbulent flame initiation and propagation through an air-fuel drop-fuel spray system is numerically modeled. The present work forms an extension of the laminar flame propagation model (1), where a dilute spray of a single component fuel in a one-dimensional closed combustor is considered. The model employs an unsteady formulation of the problem and allows unsteady mass, momentum and heat transfer between the phases. The effect of turbulence on the gas phase is incorporated by using the time-averaged governing equations with the correlation terms being modeled through a gradient transport hypothesis. The time-dependent profiles of gas and liquid properties as well as of the turbulent quantities are obtained for homogeneous (pre-mixed) and heterogeneous mixtures. The results indicate that the characteristics of flame propagation in both homogeneous and heterogeneous mixtures are sensitive to the initial value of the k/ε, which defines a turbulence decay time, and to the chemical kinetics, which defines a turbulence generation time.

NOMENCLATURE

C_μ	Constant
C_p	Average specific heat at constant pressure
D_t	Eddy diffusivity
D	Laminar mass diffusivity
D_p	Particle diffusivity
K	Variable defined as $Tp^{(1-\gamma)/\gamma}$
k	Turbulent kinetic energy
L'	Total heat transfer per unit volume to a droplet of group i
$\dot{m}_v$	Mass vaporization rate from droplet belonging to group i
n	Number density of droplets belonging to group i
O	Order of magnitude
p	Pressure
Q	Heat released per unit mass of fuel burnt
R	Radius of droplets
T	Temperature
t_p	Particle response time
t_t	Turbulent time scale
t	Time variable
T_s	Droplet surface temperature
u	Time averaged gas phase velocity
$\tilde{u}$	Instantaneous gas phase velocity
u_ℓ	Droplet velocity
w_f	Time rate of change of the fuel mass due to chemical reaction
x	Space variable
Y_i	Mass fraction of species i

GREEK SYMBOLS

Γ	Defined as $(1-\gamma)/\gamma$
γ	Specific heat ratio
ε	Turbulent kinetic energy dissipation rate
Δx	Grid spacing in the axial direction
Δt	Grid spacing in the time direction
μ_t	Turbulent viscosity
μ	Laminar viscosity
σ_k	Constant
σ_ε	Constant
ν	Stoichiometric ratio of fuel mass to oxidizer mass
ρ	Density

SUBSCRIPTS

f	Referring to the fuel
i,j	at i^{th} grid point in x-direction and j^{th} time step
ℓ	Referring to the liquid phase
N	Referring to the neutral species
O	Referring to the oxidizer
S	Droplet surface

SUPERSCRIPTS

'	Fluctuating part of a variable
~	Instantaneous value of a variable

INTRODUCTION

The theoretical study of transient, turbulent, two-phase flow in real situations often leads to a complicated set of coupled nonlinear partial differential equations. A practical solution to these equations usually involves some simplifying assumptions as well as the need for numerical modeling. This approach has been followed by several investigators [2,3,4]. Following the same approach, a model of unsteady laminar flame initiation and propagation through an air-fuel drop-fuel spray in a one-

Contributed by the Heat Transfer Division of The American Society of Mechanical Engineers for presentation at the Winter Annual Meeting, November 16-21, 1980, Chicago, Illinois. Manuscript received at ASME Headquarters July 12, 1980.

Copies will be available until August 1, 1981.

dimensional closed combustor was recently presented[1]. A dilute poly-disperse spray of a single component fuel in a mist form was considered. The interaction between the droplets was neglected. The other important features included were: transient heating and prevaporization of the droplets, lag between gas and liquid velocities, the effect of convection by semi-empirical relations, the coupling between droplet vaporization and environmental conditions, and the use of a droplet ignition criterion based on the concept of ignition Damköhler number as derived by Law[5]. The initial gas and liquid phase properties were specified in an ad hoc but consistent manner. The ignition was simulated by an imposed increase of temperature and an associated decrease in fuel and oxidizer concentrations in a small zone at one end of the combustor. Under appropriate conditions, a flame was found to establish and to propagate across the combustor. All the details and the results of the laminar flame propagation model can be found in reference (1).

The laminar flame model is now extended to include the effect of turbulence. The governing equations used for the laminar case are time-averaged which introduces the undetermined correlation terms. If the density fluctuations are disregarded, these correlations are of second order. In order to solve this closure problem, a gradient transport hypothesis, as suggested by Boussinesq[6], is used. The resulting turbulent diffusivity is determined by employing the two-equation model of turbulence[6], i.e., from the solution of transport equations for the turbulent kinetic energy (k) and the energy dissipation rate (ε). A similar treatment of the instantaneous liquid phase equations will introduce the concept of droplet or particle diffusion. It is hypothesized that the ratio of gas phase diffusivity and particle diffusivity (which is like a Prandtl number for the particle diffusivity) depends solely on the ratio of a particle response time and a characteristic turbulent eddy time. Using this hypothesis and the Stoke's drag law, the particle diffusivity is found to be a function of (a) particle mass density/gas phase mass density, (b) square of the ratio of the particle size and the turbulent length scale and (c) turbulent diffusivity/laminar diffusivity. It is argued that if the turbulent diffusivity is two or more orders of magnitude higher than the laminar diffusivity, the particle diffusivity may be neglected. For the present calculations also, the particle turbulence is neglected though its inclusion is straightforward.

As the equation for k would indicate, combustion is the only turbulence-generating mechanism in the present model. The influence of turbulence on vaporization and combustion is considered only in an indirect way; i.e., the turbulence changes the transport rates which will influence the local values of the mean flow variables and thus will influence the vaporization and chemical reaction rates. To include the direct effect of turbulence, one needs to consider how the chemical reaction and vaporization rates are influenced by the turbulence-induced fluctuations in composition, temperature, and density.

One could indicate several discrepancies in the use of this type of modeling in flows involving turbulent combustion. For example, the assumptions of gradient transport, of incompressible turbulence behavior and of unimportance of direct effects of turbulence on reaction and vaporization rates remain open to question[7,8]. The major justification for our approach is that the problem at hand is made amenable to a practical treatment. Moreover, the use of k - ε model has been used, rather successfully, in the calculation of single-phase combusting turbulent flows in complex geometries[9,10,11].

The derivations of the governing equations, the solution procedure and the numerical results are discussed in the following sections. Since the present work is an extension of the laminar flame propagation model[1], reference (1) has been very frequently cited for detailed documentation.

THE GOVERNING EQUATIONS

The assumptions used in reference (1) are also applicable to the present case. If one considers the instantaneous flow variables, one can use the same set of gas phase and liquid phase equations as given in reference (1). However, the instantaneous flow variables are now decomposed into a time-dependent mean and a fluctuating quantity as:

$$\begin{aligned} \tilde{u} &= u + u' \\ \tilde{\rho} &= \rho \\ \tilde{p} &= p + p' \\ \tilde{T} &= T + T' \\ \tilde{Y}_i &= Y_i + Y_i' \\ \tilde{U}_\ell &= U_\ell + U_\ell' \\ \tilde{n} &= n + n' \\ \tilde{R} &= R + R' \end{aligned} \qquad (1)$$

The assumption of incompressible turbulent behavior has been used in the above equations. These equations are substituted into the governing equations of reference (1) and a long-time average of the resulting equations is taken. As a result several correlation terms appear in the equations. The velocity correlations, with the mean flow being assumed one-dimensional, are modeled as

$$-\rho \overline{u'^2} = 2\mu_t \frac{\partial u}{\partial x} - \frac{2}{3}\mu_t \frac{\partial u}{\partial x} - \frac{2}{3}\rho k \qquad (2)$$

$$-\rho \overline{v'^2} = -\frac{2}{3}\mu_t \frac{\partial u}{\partial x} - \frac{2}{3}\rho k \qquad (3)$$

$$-\rho \overline{w'^2} = -\frac{2}{3}\mu_t \frac{\partial u}{\partial x} - \frac{2}{3}\rho k \qquad (4)$$

The summation of (2), (3), and (4) gives

$$k = \frac{1}{2}\left(\overline{u'^2} + \overline{v'^2} + \overline{w'^2}\right) \qquad (5)$$

The correlations involving the fluctuations of a scalar variable are modeled by using a gradient hypothesis, i.e.,

$$-\rho \overline{u'\phi'} = \frac{\mu_t}{\sigma_\phi}\frac{\partial \phi}{\partial x} \qquad (6)$$

where σ_ϕ is a turbulent Prandtl/Schmidt number and is assumed to be unity. The eddy viscosity μ_t is given by

$$\mu_t = C_\mu \rho k^2/\varepsilon \qquad (7)$$

Using the above relations, the equations for Y_f, Y_o, Y_n and K may be generalized into a single equation as

$$\frac{\partial \phi}{\partial t} + u \frac{\partial \phi}{\partial x} - \frac{1}{\rho} \frac{\partial}{\partial x} (\rho D_e \frac{\partial \phi}{\partial x}) = - \frac{\dot{nm}_v}{\rho} \phi + \frac{S\phi}{\rho} \qquad (8)$$

where ϕ may represent any of the aforementioned variables. It may be mentioned that T has been replaced by a variable K. This eliminates the pressure term in the energy equation (reference 1). $S\phi$ represents the source term and is given in Table 1 for each of the variables.

Table 1

ϕ	Y_f	Y_o	Y_n	K
S_ϕ	$\dot{nm}_v - \dot{w}_f$	$\frac{\dot{w}_f}{\nu}$	$\frac{\dot{w}_f(1+\nu)}{\nu}$	$\frac{1}{C_p} \dot{w}_f Q p^\Gamma - \dot{nm}_v p^\Gamma (\frac{L'}{C_p} - T_s)$

D_e is the effective diffusivity, given by

$$D_e = D + C_\mu k^2/\varepsilon \qquad (9)$$

The expressions for $\dot{m}_v$, $\dot{w}_f$, and L' are assumed to remain unchanged for the turbulent case and thus are given in reference (1). Similarly, the gas phase mass conservation, ideal gas equation as well as the equations for determining p (assumed spatially uniform) and u remain unchanged and are not repeated here. Also, the procedure to determine the droplet surface temperature is exactly the same as described in reference (1).

To complete the above set of equations, transport equations for k and ε are required. The derivation of these equations along with the assumptions involved in modeling the various correlation terms will not be discussed here (see references 6 and 10). The final form of the equations for one-dimensional mean flow is

$$\frac{\partial k}{\partial t} + u \frac{\partial k}{\partial x} - \frac{1}{\rho} \frac{\partial}{\partial x} (\rho \frac{D_e}{\sigma_k} \frac{\partial k}{\partial x})$$

$$= \frac{4}{3} D_e (\frac{\partial u}{\partial x})^2 - \frac{2}{3} k \frac{\partial u}{\partial x} - \frac{\dot{nm}_v}{\rho} k - \varepsilon \qquad (10)$$

$$\frac{\partial \varepsilon}{\partial t} + u \frac{\partial \varepsilon}{\partial x} - \frac{1}{\rho} \frac{\partial}{\partial x} (\rho \frac{D_e}{\sigma_\varepsilon} \frac{\partial \varepsilon}{\partial x})$$

$$= C_1 \frac{\varepsilon}{k} [\frac{4}{3} D_e (\frac{\partial u}{\partial x})^2 - \frac{2}{3} k \frac{\partial u}{\partial x}] - \frac{\dot{nm}_v \varepsilon}{\rho} - C_2 \frac{\varepsilon^2}{k} \qquad (11)$$

It is important to note that a term due to droplet vaporization ($\dot{nm}_v/\rho$) appears as a sink term in k and ε equations. This is because the equations are written in a non-conservation form. This term will be absent in the conservation form of k and ε equations, which means that there is no turbulence associated with the vaporization process. However, along a streamline k and ε will change due to vaporization.

It may also be mentioned that the term $-2/3\ k \cdot \partial u/\partial x$ appearing in these equations represents the effect of compressibility. For example, in case of expansion $\frac{\partial u}{\partial x} > 0$, and the effect of this term is to reduce the rate of increase of turbulent kinetic energy. The values of the constants appearing in the above equations are taken to be[10]

$$C_\mu = .09$$
$$\sigma_k = 1.0$$
$$\sigma_\varepsilon = 1.0 \qquad (12)$$
$$C_1 = 1.44$$
$$C_2 = 1.92$$

PARTICLE DIFFUSION

Gas phase turbulence can cause droplets or particles to fluctuate about some mean velocity. This gives rise to the concept of particle diffusion, which may be approximated by adding a diffusion term in the liquid phase equations. This term may be modeled as

$$\overline{n' u_\ell'} = -D_p \frac{\partial n}{\partial x} \qquad (13)$$

Several investigators have studied the phenomenon of particle diffusion. One of the earliest studies is due to Tchen[12]. Under highly restrictive conditions which are not applicable for a real case (see references 13 and 14 for details), his study indicated that the diffusion coefficients for the particle and for the gas are the same. Further studies [15,16] showed that the ratio of particle diffusivity to eddy diffusivity is a function of particle response time and both the Lagrangian and Eularian microscales of turbulence. Here it is hypothesized that the ratio of the gas phase diffusivity and the particle diffusivity D_p is solely dependent on the ratio of a particle response time and a turbulent eddy time, i.e.,

$$\frac{D_t}{D_p} = f(t_{pt}) \qquad (14)$$

where $t_{pt} = t_p/t_t$.

It is expected that if $t_{pt} \to 0$, particle diffusivity will be equal to the gas phase diffusivity. On the other hand for a very large t_{pt}, the particle diffusivity may be negligible. The particle response time may be expressed in terms of a given velocity perturbation and the particle acceleration, i.e.,

$$t_p = \frac{|u - u_\ell|}{|\frac{DU_\ell}{D_t}|} \qquad (15)$$

using Stoke's drag law for a spherical particle,

$$\frac{DU_\ell}{D_t} = \frac{9}{2} \frac{\mu}{\rho_\ell R^2} (u - u_\ell)$$

t_p can be expressed as,

$$t_p = \frac{2}{9} \frac{\rho_\ell R^2}{\mu} \qquad (16)$$

Turbulence is generally characterized by a wide range of length and time scales. Large scale turbulence may be characterized by the length and time scales associated with large size eddies which carry most of the energy. For these eddies, the characteristic length and time scales may be defined as $\ell_t = k^{3/2}/\varepsilon$ and $t_t = k/\varepsilon$. Small scale turbulence is represented by Kolmogorov's microscales[12] where the time scale is given as $t_t = (\nu/\varepsilon)^{1/2}$. In order to obtain a lower bound on t_{pt}, it is appropriate to consider the larger of the two turbulent time scales. Then using Eq. [16], t_{pt} can be written as

$$t_{pt} = \frac{2}{9}\frac{\rho_\ell R^2 \varepsilon}{\mu k}$$

which can be rewritten as

$$t_{pt} = \frac{2}{9C_\mu}\frac{\rho_\ell}{\rho}\frac{R^2}{\ell_t^2}\frac{\nu_t}{\nu} \qquad (17)$$

According to Eq. (17), the particle diffusivity depends on (a) particle mass density/gas phase mass density, (b) square of the ratio of particle size and a turbulent eddy size and (c) turbulent diffusivity/laminar diffusivity. Generally, the liquid density is two to three orders of magnitude higher than the gas density. If the turbulent diffusivity is one to two orders of magnitude higher than the laminar one, then for droplets of not too small a size (say for droplet diameter of more than 40 microns), t_{pt} will usually be quite large. Under those conditions, one can assume that the particle diffusion is negligible. It is worth noticing that $t_{pt} \to \infty$ corresponds to the case considered by Tchen[12]. It may also be mentioned that the inclusion of particle diffusivity will tend to give a parabolic character to the liquid phase equations which are hyperbolic, otherwise. The task of including the particle diffusion is being pursued by the present authors. At the moment, the particle diffusivity is neglected. Then the liquid phase equations are the same as given in reference (1).

SOLUTION PROCEDURE

The solution procedure used here is more or less the same as described in reference (1). The nondimensionalization and the linearization of the governing equations are obtained in the same manner. The appropriate boundary conditions for the gas phase and the liquid phase variables are also described in reference (1). For k and ε equations, the following boundary conditions are used:

$$\frac{\partial k}{\partial x} = 0$$

near the combustor ends

$$\frac{\partial \varepsilon}{\partial x} = 0$$

It must be noted that the above relations are applied "near" but not "at" the wall.

The linearized equations are replaced by finite-difference approximations by employing an implicit scheme, similar to Crank-Nicolson scheme. This leads to a tridiagonal matrix for each of the gas phase variables Y_f, Y_o, Y_n, K, k, and ε. For the liquid phase equations, the first spatial derivative is approximated as

$$\left(\frac{\partial Y}{\partial x}\right)_{i,j+1/2} = \frac{Y_{i,j+1} - Y_{i-1,j+1} + Y_{i+1,j} - Y_{i,j}}{2\Delta x} + O(\Delta t \cdot \Delta x) \qquad (18)$$

where i and j represent, respectively, the iΔx and jΔt locations in space and time. This yields an explicit solution of the liquid phase variables. The initial conditions for the gas phase as well as for the liquid phase variables are provided in an ad hoc but self-consistent manner. The flame initiation is modeled by imposing an increase in gas temperature and a decrease in fuel and oxidizer concentrations in a small zone at the left end of the combustor. The details of this model are given in reference (1).

RESULTS

Calculations have been made for turbulent flame propagation in homogeneous, as well as heterogeneous, mixtures of air and normal decane fuel. In both the cases, the initial conditions are identical except that in the homogeneous case, fuel is present in the vapor form. The initial pressure is one atmosphere, and the overall equivalence ratio is 0.95. Several computer runs have been made with initial k and ε values being different in each run. The variables are plotted versus spatial position for different times to indicate the propagation of flame. The profiles at t = 0 represent the initial conditions.

Results of two runs (P_1 and P_2) for the turbulent flame in homogeneous mixtures are shown in Figs. 1 and 2. The only difference in the two runs is in the initial values of k and ε (see Table 2). Profiles of temperature, fuel, and oxidizer mass fractions in Figs. 1a to 1c clearly indicate a propagating flame. Figure 1d gives the gas velocity profile at t = 60 ms. The gas expansion caused by heat release as a result of chemical reaction is quite evident there. One of the more notable features of runs P_1 and P_2 is demonstrated by Figs. 1e, 1f, and 2b. As indicated by these figures and further substantiated by Table 2, the profiles of k and ε at later times are very sensitive to the initial k/ε ratio which represents a turbulence decay time. This may be explained by examining the production and dissipation terms in k (or ε) equation. If the laminar diffusivity is neglected, using Eq. (10), the source terms for the turbulent energy for the pre-mixed case ($\dot{m}_v = 0$) can be written as

$$S_k = P_k - \varepsilon \qquad (19)$$

where P_k, the production term, is

$$P_k = \frac{2}{3} k \frac{\partial u}{\partial x}\left(0.18 \frac{\partial u}{\partial x}\frac{k}{\varepsilon} - 1\right) \qquad (20)$$

Since ∂u/∂x term is mainly determined by the heat release due to chemical reaction, it is significant only in the flame region. As a result, as indicated by Fig. 1e, k increases across the flame. However, the overall k value throughout the combustor shows an initial decrease. This is due to the fact that it takes a finite time (similar to ignition delay time) for a propagating flame to become established. During that time, ∂u/∂x is relatively small and as a result, the turbulence decay term (ε) dominates the turbulence production term. After that initial period, k starts increasing with time (see Fig. 1e

and Table 2). The turbulent energy dissipation rate follows the same behavior.

TABLE 2

Time t (ms)		0	5	10	20	30	40	60
Run P_1 (400, 2000)	k^*	1	.98	.96	.84	1.1	1.17	5.48
	ϵ^*	1	.96	.93	.88	1.08	1.13	5.13
Run P_2 (400, 8000)	k^*	1	.91	.84	.60	.63	.56	.47
	ϵ^*	1	.86	.72	.53	.42	.33	.23
Run T_1 (400, 2000)	k^*	1	1.02	.97	1.45	2.23	4.75	
	ϵ^*	1	1.02	.93	1.68	2.5	14.4	
Run T_2 (400, 8000)	k^*	1	.92	.84	.72	.68	.62	.52
	ϵ^*	1	.84	.72	.54	.52	.38	.24
Run T_3 (100, 500)	k^*	1	1.08	1.14	1.29	1.71	2.0	
	ϵ^*	1	1.12	1.21	1.44	2.04	2.27	
Run T_4 (6400, 512000)	k^*	1	.72	.52	.32	.26	.20	
	ϵ^*	1	.54	.3	.12	.07	.05	

k^* and ϵ^* are, respectively, the maximum values of k and ϵ normalized by their initial values. Runs P_1 and P_2 are for the homogeneous case, whereas runs T_1, T_2, T_3, and T_4 are for the heterogeneous case. The values in the parenthesis are, respectively, the initial k and ϵ values for each run.

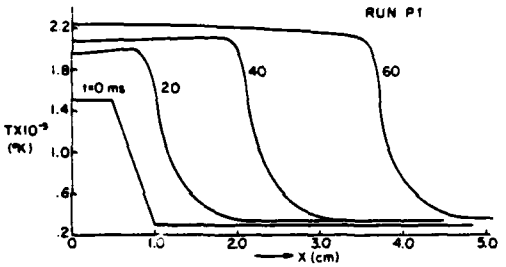

TEMPERATURE PROFILES
Fig.1a

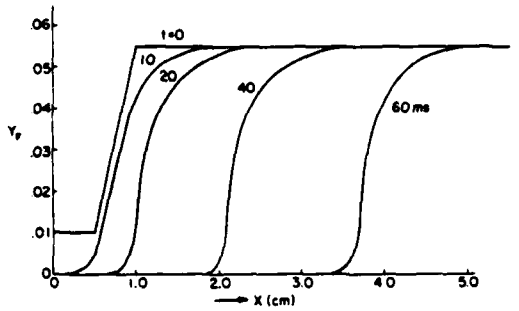

FUEL MASS FRACTION PROFILES
Fig.1b

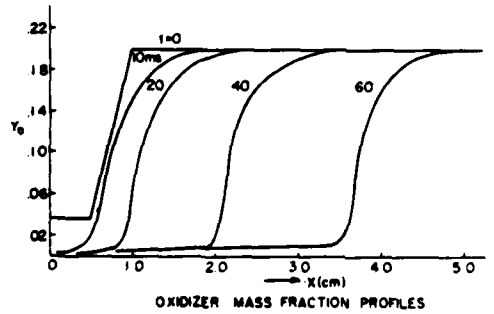

OXIDIZER MASS FRACTION PROFILES
Fig.1c

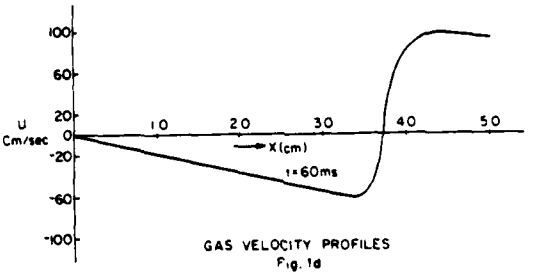

GAS VELOCITY PROFILES
Fig. 1d

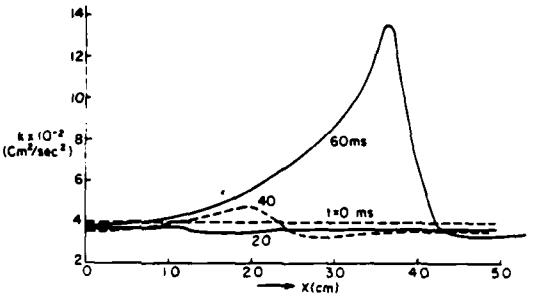

TURBULENT KINETIC ENERGY PROFILES
Fig 1e

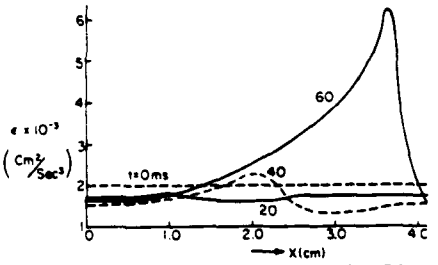

TURBULENT KINETIC ENERGY DISSIPATION F
Fig.1f

The results of run P_2 tell quite a different story. As indicated by Fig. 2b, the values of k and ϵ not only decrease monotonically with time, but they show an additional dip in the flame region. This occurs since, for this run, the production term P_k becomes negative in the flame region. According to Eq. (20), the sign of this term depends on the relative amplitudes of k/ϵ (turbulence decay time) and $\partial u/\partial x$, related to the inverse of the chemical reaction time. For example, the value of $\partial u/\partial x$ is more or less the same for runs P_1 and P_2 as the chemical kinetics is identical for these runs. However, the initial k/ϵ in run P_2 was four times smaller than that in run P_1. As a result, k increases across the flame in run P_1 and decreases across the flame in run P_2. The dissipation rate (ϵ) follows the same behavior. Hence, the profiles of k and ϵ are mainly determined by the turbulence decay time, defined by k/ϵ, and the turbulence generation time, defined by the inverse of the chemical reaction rate. As a result, these two time scales greatly influence the turbulent flame propagation. It may also be noted that the change of sign for the production term in the above case is directly attributed to the inclusion of compressibility effect in the turbulent modeling.

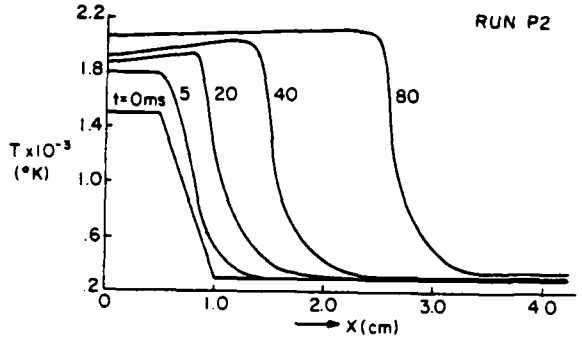

TEMPERATURE PROFILES
Fig. 2a

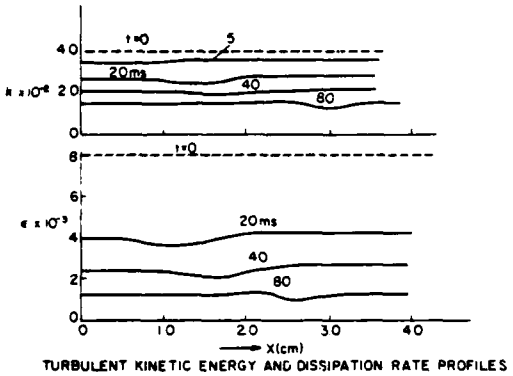

TURBULENT KINETIC ENERGY AND DISSIPATION RATE PROFILES
Fig 2b

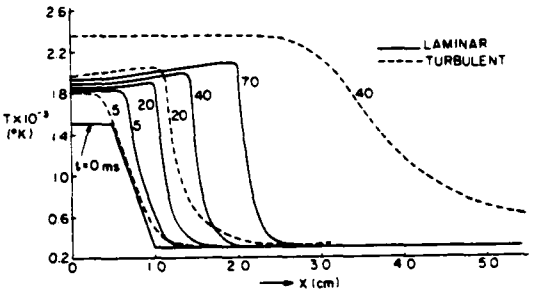

GAS TEMPERATURE PROFILES
Fig 3a

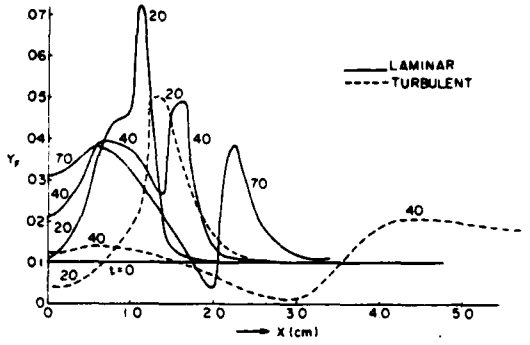

FUEL VAPOR MASS FRACTION PROFILES
Fig 3b

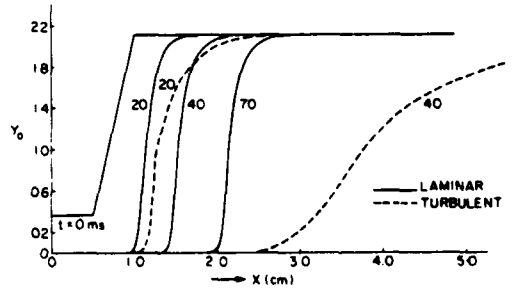

OXIDIZER MASS FRACTION PROFILES
Fig 3c

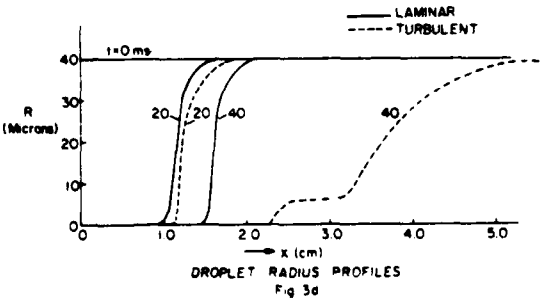

DROPLET RADIUS PROFILES
Fig 3d

Results of flame propagation in a heterogeneous mixture are given in Figs. 3 to 6. Figure 3 gives the results for laminar as well as turbulent flame propagation. It may be mentioned that the laminar results, reported here, are obtained from the present turbulent code by taking turbulent diffusivity to be zero. These results are identical to those reported in reference (1). It is noteworthy that inspite of the identical initial conditions, the flame initiation process is different in the laminar and turbulent cases. The flame initiation time (similar to an ignition delay time) is controlled by chemical and diffusion processes (convection is absent initially). Because of the higher diffusion, it takes longer for a propagating flame to become established in the turbulent case (see gas temperature profiles at t = 5 ms in Fig. 3a). Once it starts propagating, the turbulent flame moves faster than the laminar one. The expected features, like increased flame speed and thickness for the turbulent case, are quite evident in Figs. 3a to 3e. The typical values are

	LAMINAR	TURBULENT
Diffusivity in the flame region	1.5 cm^2/sec	15 cm^2/sec
Flame Speed	20 cm/sec	80 cm/sec
Flame Thickness	0.5 cm	1.5 cm

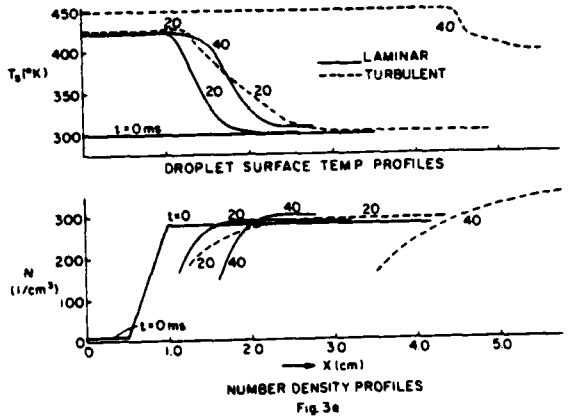

Fig. 3a

For both cases, Fig. 3b indicates two peaks in the fuel vapor mass fraction profiles. The first peak represents a fuel high zone left behind a pre-mixed type propagating flame, represented by the second case. Because of the higher diffusion, the peaks for the turbulent case are not as sharp and as high as for the laminar case. Also, the phenomenon of a secondary diffusion flame (see reference 1) seems to be absent for the turbulent case. For the laminar case, the secondary flame appears after t = 100 ms and is not shown here. The profiles of liquid phase properties are shown in Figs. 3d and 3e. Two points are worth mentioning: (i) In spite of the fact that the particle diffusivity is assumed to be zero, the liquid phase properties show, relatively, a smooth variation for the turbulent case. (ii) The higher droplet surface temperature in the hot region of the combustor for the turbulent case is due to the higher pressure, since at a given time, more mass has been burnt for the turbulent case.

The results of three more runs for the turbulent case are shown in Figs. 4 to 6. All the four turbulent runs (runs T_1, T_2, T_3, and T_4) differ from each other only in their initial k and ε values. Other initial conditions as well as the chemical kinetics are identical. The notable feature of these four runs is that the turbulent flame propagation is greatly influenced by the initial k/ε values. Depending on the initial k/ε value (and the chemical kinetics), one can have an accelerating or decelarating flame. Coupled to this is the fact that depending on k/ε and chemical kinetics (through $\partial u/\partial x$ term), the turbulence can increase or decrease across the flame. This is substantiated by the values in Table 2, where the maximum values of k and ε, normalized by their respective initial values, as functions of time are tabulated. Moreover, as these values indicate, the time rate of increase (or decrease) of k and ε is a function of the initial k/ε value. For run T_4, initial k/ε value is 12.5 as compared to a value of 50 for run T_2. The values of k and ε decrease relatively faster in run T_4 as compared to run T_2. It may also be noted that for run T_1, the maximum values of k and ε first decrease and then increase, whereas for run T_3, these increase monotonically. This is due to the higher initial diffusivity for run T_1. Because of higher diffusion, it takes longer for a flame to get initiated in run T_1. This causes the turbulence production term to be initially smaller than the dissipation term for run T_1. A similar situation has been mentioned for the pre-mixed case.

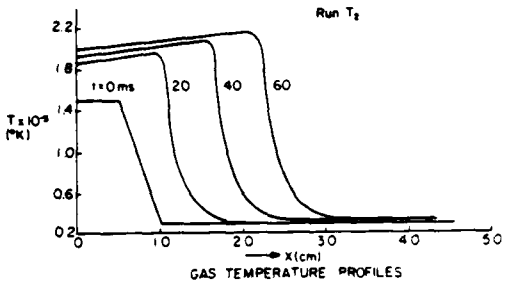

Fig 4a

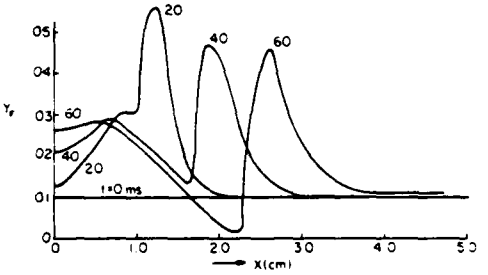

Fig 4b

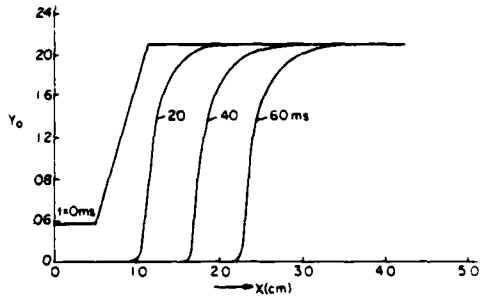

Fig 4c

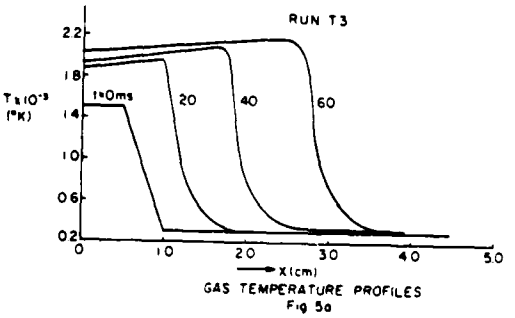

Fig 5a

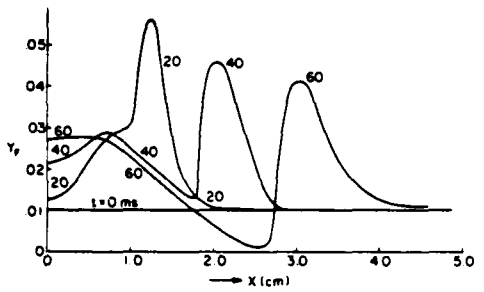

FUEL VAPOR MASS FRACTION PROFILES
Fig 5b

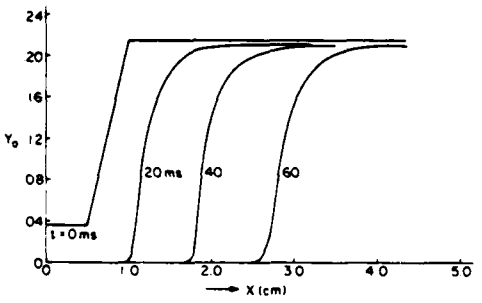

OXIDIZER MASS FRACTION PROFILES
Fig 5c

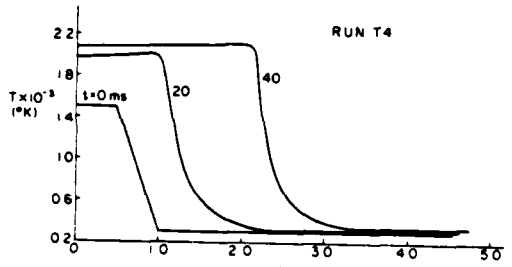

GAS TEMPERATURE PROFILES
Fig. 6a

Some additional gross features of the turbulent flame propagation for all the runs are summarized in Table 3. It may be worth noting that in runs T_3 and T_4, the flame speed and thickness are roughly the same. This is in spite of the fact that initial diffusivity in run T_4 is four times higher than that in run T_3. Again, the reason is that the turbulence level increases in run T_3 and decreases in run T_4.

All of the aforementioned computer runs have been made on DEC-20 system. In order to limit the computation costs, in almost all the runs, computation has been terminated when flame traverses half the combustor length. On DEC-20 system, this takes typically 90 minutes of computer time, which is equivalent to about 30 minutes on relatively faster systems (say IBM 360). In all the runs, the step sizes in space and time were, respectively, 1.25 mm and 0.01 ms. These values were required to resolve the combustor process, i.e., the flame thickness and the reaction rate.

TABLE 3

Run	(k/ε initial (ms)	t_c (ms)	(σ_t) initial	Flame	S_f (cm/sec)	δ_f (cm)
P_1	200	.25 to 10	7.2	Accelerates	100	1.5
P_2	50	.25 to 10	1.8	Decelerates	25	6
T_1	200	25 to 10	7.2	Accelerates	80	1.5
T_2	50	.25 to 10	1.8	Decelerates	40	.75
T_3	200	.25 to 10	1.8	Accelerates	50	90
T_4	12.5	25 to 10	7.2	Decelerates	60	90

t_c = chemical reaction time

S_f = typical flame speed

δ_f = typical flame thickness

SUMMARY AND CONCLUSIONS

The main findings of the present study may be summarized as follows:

1. The laminar flame propagation model of reference (1) has been successfully extended to predict the gross features of turbulent flame propagations in air-fuel drop-fuel vapor mixtures in a one-dimensional combustor. The turbulence model used is based on the gradient transport hypothesis, where the eddy diffusivity is determined by solving the transport equations for k and ε.
2. By a simple consideration of a particle response time and a turbulent eddy time, an estimate is made for the order of magnitude of particle diffusivity. It is shown that the ratio of particle diffusivity to gas phase turbulent diffusivity depends on (a) particle mass density/gas phase mass density, (b) square of the ratio of a particle size to a turbulent eddy size, and (c) turbulent diffusivity/laminar diffusivity. Conditions are discussed where the particle diffusivity may be neglected. It is neglected presently but can be included in a future study.
3. The characteristics of turbulent flame propagation in both homogeneous and heterogeneous mixtures seem to be highly sensitive to the relative magnitudes of k/ε, which defines a turbulence decay time, and inverse of the chemical reaction rate, which defines a turbulence generation time. This conclusion should be examined more generally by further numerical studies and experimental results.
4. The present model has been used for a mono-dispersed spray. The poly-disperse spray can be considered in a future study.

ACKNOWLEDGMENTS

The authors gratefully acknowledge the financial support of Army Research Office and Department of Energy for this work.

REFERENCES

1 Seth, B., Aggarwal, S. K. and Sirignano, W. A., "Flame Propagation Through an Air-Fuel Spray Mixture with Transient Droplet Vaporization," to appear in Combustion and Flame.

2 Polymeropoulos, C. E., "Flame Propagation in a One-Dimensional Liquid Fuel Spray," Combustion Science and Technology, Vol. 9, 1974.

3 Dukowicz, J. K., "A Particle-Fluid Numerical Model for Liquid Sprays," Los Alamos Scientific Laboratory, Report LA-UR-78-3304, Los Alamos, New Mexico.

4 Gosman, A. D. and Johns, R. J. R., "Computer Analysis of Fuel-Air Mixing in Direct-Injection Engines," Paper 800091 presented at the SAE Congress and Exposition, Detroit, Michigan, 1980.

5 Law, C. K., "Chemical and Physical Processes in Combustion," The Eastern Section of the Combustion Institute, East Hartford, November 10-11, 1977.

6 Launder, B. E. and Spalding, D. B., Mathematical Models of Turbulence, Academic Press, New York, 1973.

7 Libby, P. A. and Bray, K. N. C., AIAA 18th Aerospace Sciences Meeting, Pasadena, California, 1980.

8 Williams, F. A. and Libby, P. A., AIAA 18th Aerospace Sciences Meeting, Pasadena, California, 1980.

9 Syed, S. A. and Bracco, F. V., "Further Comparisons of Computed and Measured Divided-Chamber Engine Combustion," Paper 790247 presented at the SAE Congress and Exposition, Detroit, Michigan, 1979.

10 Ramos, J. I., "Axisymmetric Flow Fields in Motored and Firing, Spark-Ignition Engines," Ph.D. Thesis, Department of Mechanical and Aerospace Engineering, Princeton University, Princeton, New Jersey, 1980.

11 Gosman, A. D. and Johns, R. J. R., "Development of a Predictive Tool for In-Cylinder Gas Motion in Engines," Paper 780315 presented at the SAE Congress and Exposition, Detroit, Michigan, 1978.

12 Tchen, C. M., Dissertation, Delft, Martinus Nijhoff, The Hague, 1947.

13 Soo, S. L., Fluid Dynamics of Multiphase Systems, Blaisdell, Waltham, Massachusetts, 1967.

14 Hinze, J. O., Turbulence, McGraw-Hill Book Company, 1975.

15 Lumley, J. L., Journal of Math. Phys., 3 (2), 309, 1962.

16 Peskin, R. L., "The Diffusivity of Small Suspended Particles in Turbulent Fluids," presented at the National Meeting, A.I.Ch.E., Baltimore, 1962.

17 Tennekes, H. and Lumley, J. L., A First Course in Turbulence, The MIT Press, Cambridge, Massachusetts, 1972.

81-WA/HT-46

THE AMERICAN SOCIETY OF MECHANICAL ENGINEERS
345 E 47 St., New York, N.Y. 10017

Effect of Numerical Modeling on One-Dimensional Enclosed Homogeneous and Heterogeneous Deflagrations

S. K. Aggarwal

W. A. Sirignano

Mechanical Engineering Department,
Carnegie-Mellon University,
Pittsburgh, PA

The objective of this study is to evaluate the effectiveness of several finite difference techniques in modeling unsteady homogeneous and heterogeneous flames in closed combustors. The problem of propagation of a pre-mixed homogeneous flame and a heterogeneous flame in air-fuel droplet-fuel vapor mixture is formulated. The governing equations have been solved by using four different numerical techniques. For the pre-mixed case, flame propagation is computed for two fuels, propane and n-octane. For the two-phase heterogeneous case, n-octane fuel is used. The results are obtained in terms of the profiles of gas and liquid phase properties at different instances of time as the flame traverses the combustor. From these results, the relative efficiency and accuracy of each of the numerical techniques is discussed.

INTRODUCTION

Numerical computation of unsteady flows with combustion, where the flow properties are assumed to vary in one or two spatial directions, have reached an advanced level of sophistication. Both explicit and implicit methods have been used to a variety of flow situations. Generally, the implicit numerical methods have been recommended because of their favorable stability properties. The explicit schemes for a parabolic unsteady PDE are required to satisfy certain stability requirements, which impose a restriction on the temporal step size relative to the spatial mesh size. In one-dimensional problems, these stability conditions are expressed at $\Delta t \leq \Delta x/|u|+c$ and $t \leq \Delta x^2/2\vartheta$. Thus, the maximum allowable time step could be dictated by the spatial mesh size, rather than by a characteristic time of a physical process under consideration. Since the implicit methods are generally* free from these restrictions, it may be possible to use a relatively larger time step than what is permissible in explicit schemes. However, the advantage of using an implicit formulation may prove illusory in many practical situations. An implicit scheme requires a relatively larger number of arithmetic operations than an explicit scheme. For example, as discussed by Cheng [3], the solution of a scalar PDE will require five times more computational effort per time step in an implicit formulation than in an explicit one. For a coupled non-linear PDE set, the implicit formulation will be even more time consuming because an iterative scheme is required to take care of the non-linearities and the coupling in the governing equations. As a result, an implicit method can retain its computational advantage only if the time step is considerably larger (say an order of magnitude and higher) than that allowed by stability requirements.

In an effort to make the implicit formulation more efficient, several linearization techniques have been developed. These techniques mainly fall into two categories. One is the quasi-linearization (Newton-Raphson) iterative process as originally suggested by Bellmann and Kalaba [1], and later used by Sharma and Sirignano [4] for solving a non-linear PDE set. In this method, which requires the solution of a tridiagonal matrix for each of the scalar equations, the linearization is conducted by using a Taylor expansion in an iterative space. The second class of linearization processes has been suggested independently by Briley and McDonald [2] and Lindenmuth and Killer [5]. The technique, which has been called a time-linearization, uses a Taylor expansion in time and requires the solution of a block tri-diagonal system as opposed to a simple tri-diagonal system in quasi-linearization scheme. The main attraction of the time-linearization method over the quasi-linearization method is that the former leads to a non-iterative algorithm. However, for any of these implicit linearization methods to have an edge over the explicit schemes, the temporal step-size still has to be at least an order of magnitude larger than the maximum permissible in the explicit schemes. On the other hand, there are many practical situations where the space and time step restrictions imposed due to the finite differencing of the governing equations are not as important as those imposed by the physical and chemical processes under consideration. In such cases, the advantages of even highly efficient implicit schemes become questionable. The physical situation considered in the present study falls into this

*Still, implicit schemes are required to satisfy a cell Reynolds number criterion and any stability conditions arising from the implementation of boundary conditions.

Contributed by the Heat Transfer Division of THE AMERICAN SOCIETY OF MECHANICAL ENGINEERS for presentation at the Winter Annual Meeting, November 15-20, 1981, Washington, D.C. Manuscript received at ASME Headquarters July 13, 1981.

Copies will be available until August 1, 1982.

category.

An unsteady propagation of pre-mixed homogeneous flames as well as of heterogeneous flames in an air-fuel droplet-fuel vapor mixture in enclosed, one-dimensional combustors is formulated. For the pre-mixed homogeneous case, the set of parabolic PDE's is solved by four different finite-difference schemes; an explicit approach, an iterative sequential implicit method without any formal linearization, an iterative quasi-linearization implicit method with a scalar tri-diagonal matrix system and a non-iterative time-linearized implicit technique with a block tri-diagonal matrix. In each of the four methods, a central or upwind difference scheme is used for the spatial derivatives, depending upon the local cell Reynolds number. The relative merits of each of the numerical techniques is discussed.

For the case of heterogeneous flame propagation in a two-phase flow, the gas-phase equations, a subset of parabolic PDE's, is again solved by the same four numerical techniques. The liquid phase equations, a subset of hyperbolic PDE's, is solved explicitly. It is, however, worth mentioning that because of the coupling between the two sets, all the implicit schemes require iteration and, in each iteration, the liquid phase properties, although obtained explicitly, are updated. In the next section, the physical model and governing equations are presented. This is followed by the discussion of the solution procedure employed in each of the methods. Finally, the results are presented and the relative merits of the various numerical techniques are discussed.

PHYSICAL MODEL AND GOVERNING EQUATIONS

The physical situation considered in the present study is that of a one-dimensional combustor, enclosed at both ends for both the pre-mixed and the heterogeneous two-phase cases. The initial profiles of the gas phase properties, as well as of the liquid phase properties, are prescribed (see Figures 1-10). The conservation of gas phase properties is described by the following equations:

$$\partial\rho/\partial t + \partial/\partial x\,(\rho u) = S_\rho \tag{1}$$

$$\rho\ \partial Y_i/\partial t + \rho u\ \partial Y_i/\partial x - \partial/\partial x\,(\mu\ \partial Y_i/\partial x) = S_i \tag{2}$$

$$\rho\partial\phi/\partial t + \rho u\ \partial\phi/\partial x - \partial/\partial x\,(\mu\partial\phi/\partial x) = S_\phi \tag{3}$$

$$Y_n = 1 - \sum_{i=1}^{n-1} Y_i \tag{4}$$

$$p^{1/\gamma} = \rho R\phi \sum_{i=1}^{n} Y_i/W_i, \text{ where } \phi = Tp^{1-\gamma/\gamma} \tag{5}$$

$$\int_0^L \partial\rho/\partial t\ \Delta x = \int_0^L S_\rho\ \Delta x \tag{6}$$

$$(\rho u)_x = (\rho u)_{x=0} + \int_0^x (S_\rho - \partial\rho/\partial t)\Delta x \tag{7}$$

where ρ, u, T, p and Y_i are respectively the density, velocity, temperature, pressure and mass fractions for the gaseous phase. Furthermore, μ, R, γ and W_i are the gas viscosity, universal gas constant, ratio of specific heats, and molecular weight for species i. Also, x and t are the spatial and temporal coordinates and L is the combustor length. S_ρ, S_i, and S_ϕ are the source or sink terms for the gas phase and are prescribed in Table 1. These are discussed in greater detail in [6]. In deriving the above equations, it is assumed that:

1. the volume occupied by the liquid phase is negligible,
2. pressure is only a function of time,
3. the species diffusion follows Fick's law with equal mass diffusivities for all species,
4. Prandtl and Schmidt numbers are unity,
5. radiative heat transfer is negligible,
6. viscous dissipation is negligible and the gas kinetic energy is small as compared to its thermal energy,
7. gas phase is thermally and calorically perfect with equal, constant specific heat, and
8. the gas phase chemical reaction is governed by a single-step second-order kinetics.

LIQUID-PHASE EQUATIONS

The major assumption in describing the liquid phase is that the droplet properties are described by an Eulerian approach. Further, a single component mono-disperse dilute fuel spray is considered. As a result, the interactions between the droplets are neglected. The droplets are assumed to be spherical with the convection effect being described by a Ranz-Marshall correlation [7]. Furthermore, the droplet interior temperature is considered uniform. This is equivalent to a large liquid thermal conductivity assumption. The derivation of source (or sink) terms for the gas and liquid phases are based on this assumption. Then, the subset of hyperbolic PDE's for the liquid-phase properties are:

$$\partial n/\partial t + \partial/\partial x\,(n\ u_\ell) = 0 \tag{8}$$

$$\partial S/\partial t + u_\ell\ \partial S/\partial x = -\dot{m}/2\pi R_\ell\rho_\ell \tag{9}$$

where $S = R_\ell^2$

$$\partial u_\ell/\partial t + u_\ell\ \partial u_\ell/\partial x = 3/8\ C_D\ \rho/\rho_\ell\ R_\ell|u-u_\ell|(u-u_\ell) \tag{10}$$

$$4/3\pi\ R_\ell^3\rho_\ell\ C_{p_\ell}\ [\partial T_\ell/\partial t + u_\ell\ \partial T_\ell/\partial x] = \dot{m}(L'-L) \tag{11}$$

$$C_D = 27/\ R_{e_\ell}^{.8} \tag{12}$$

$$Y_{fs} = 1/[1+W_o/W_f(p/p_v - 1)] \tag{13}$$

$$p_v = (1/760)(\exp[A_\ell - B_\ell/(T_\ell + C_\ell)] \tag{14}$$

where n, u_ℓ, R_ℓ, and T_ℓ are respectively, the droplet number density, velocity, radius, and surface temperature. Furthermore, ρ_ℓ and C_{p_ℓ} are the density and specific heat for the liquid fuel. The equilibrium vapor fuel mass fraction (Y_{fs}) as a function of T_ℓ is prescribed by Antoine's relation (13,14) as discussed

in [8]. Finally, the drag law (12) is used in a form suggested by Ingebo [9].

It is noteworthy that in spray combustion studies, the controversy regarding the existence of envelope flame surrounding the individual droplets still exists. The experimental studies by Chigier [10] show no evidence of individual droplet flames. However, under certain conditions such as large droplets in hot surroundings, the existence of an envelope flame is a distinct possibility. In the present study both of the cases are considered, where the presence of a droplet envelope flame is determined by a critical Damköhler number as used by Law [11].

NUMERICAL CONSIDERATIONS AND SOLUTION PROCEDURES

Here we describe the method of solution for each of the numerical schemes. The computer codes have been developed in such a way that the same code can be used for the pre-mixed single-phase and heterogeneous two-phase flames. The pre-mixed case is recovered from the two phase case by changing the initial conditions and making S_o identically equal to zero. Therefore, the solution procedure is outlined only for the latter case. In all the numerical schemes, the general procedure is as follows:

First of all, the liquid-phase properties are advanced in time explicitly by using the gas and liquid phase properties at the known time level. Since the liquid-phase equations are hyperbolic in nature, the spatial derivatives are finite differenced by using an upwind scheme. The advanced-liquid phase properties are then used to integrate the gas-phase energy and species conservation equations. In all the numerical schemes, the convection term in the gas-phase equations is finite-differenced by using a central or upwind scheme as determined by the local cell Reynolds number. At locations where the cell Reynolds number exceeds two, the difference approximation is changed from central to upwind [12]. The values of ϕ and Y_i obtained at the advanced time level are then employed in (5,6) to obtain new gas pressure and density. Finally, Eq. (7) is used to give the new gas velocity and the whole cycle is repeated to advance to the next time-step.

The gas-phase equations are solved by using four different numerical schemes. In the explicit schemes, the solution is advanced by using the spatial differencing at the explicit time-level. In the fully implicit scheme, there is no formal linearization. The finite differencing of the spatial derivative is written at the implicit time level. The finite-difference form is assumed to be linear and the solution is obtained by inverting the tri-diagonal matrix. The equations are solved in a sequential manner. First of all, the energy equation is solved, which provides an updated value of ϕ, which in turn is used for solving the equation for Y_f. Then updated values of ϕ and Y_f are used to solve for Y_O. This procedure of sequential updating is continued in an iterative manner until the desired convergence is obtained and the cycle is repeated to advance the solution to the next time-step.

In the implicit method with quasi-linearization in an iterative space, the linearization procedure can be described by considering any of the governing equations as:

$$\partial\psi/\partial t = z(\psi, \psi_x, \psi_{xx}) \qquad (15)$$

where ψ stands for any of the variables and subscript x denotes the spatial derivative.

Equation (15) is linearized as:

$$(\partial\psi/\partial t)^{n+1} = z^n + (\partial z/\partial\psi)^n \Delta\psi^{n+1} + (\partial z/\partial\psi_x)^n \Delta\psi_x^{n+1} + (\partial z/\partial\psi_{xx})^n \Delta\psi_{xx}^{n+1} \qquad (16)$$

$$\text{where } \Delta\psi^{n+1} = \psi^{n+1} - \psi^n \qquad (17)$$

Finite differencing of (16), along with the boundary conditions (no heat and mass diffusion at the combustor boundaries) yields a tridiagonal matrix for each of the variables. The method still requires iteration because the governing equations are coupled. The idea of using the quasi-linearization process over the straight forward implicit scheme without any formal linearization is to expedite the convergence process.

The time-linearization non-iterative formulation is described in detail by Briley and McDonald [2]. Only a brief description of the technique is given here. For a first order non-linear equation

$$(\partial Y/\partial t)^{n+1} = F(Y)\ \partial/\partial x\ G(Y) \qquad (18)$$

the Taylor series expansion of non-linear terms in time is written as

$$(\partial Y/\partial t)^{n+1} = (FG_x)^n + [F^n(\partial G_x/\partial Y)^n + G_x^n\ (\partial F/\partial Y)^n]\ (Y_i^{n+1} - Y_i^n)/\Delta t \qquad (19)$$

The non-linear source terms and the second order spatial derivative terms are treated in the same way. Using an appropriate finite differencing and the boundary condition leads to a tridiagonal matrix. For a coupled set of non-linear equations (i.e., when Y is a column vector), the above linearization process will result in a block tri-diagonal system, which can be solved either by a standard block tri-diagonal system solver or by a band matrix solver. The block tri-diagonal algorithm is similar to that used for solving a scalar tri-diagonal system except that each element itself becomes a square matrix. The band matrix solver is a more efficient way of inverting a block tri-diagonal matrix, where all the diagonals in the block tri-diagonal system are transformed to form another matrix and the solution is obtained by inverting the transformed matrix. It may be mentioned that in the present calculations, the band matrix solver was fifty percent more efficient than the block tri-diagonal matrix solver.

RESULTS AND COMPARISONS OF NUMERICAL SCHEMES

The results for the heterogeneous flame propagations in air-fuel vapor-fuel droplet (n-octane) mixture in a one-dimensional enclosure combustor of length 10cm are presented in Figures 1-10. To keep the computer costs under control, computations have been made until the flame traverses about half the combustor length. In addition, for the purpose of clarity, the profiles of the various gas and liquid-phase properties are plotted for only half the length. The initial profiles (at t=0) of all the gas and liquid-phase properties are assumed uniform except that a flame initiation or ignition source of length 0.5cm and of temperature 1500°K is provided near the

left end of the combustor. The initial value of all variables are varied linearly from the hot zone values to ambient values in the next 0.5cm to avoid large gradients near the ignition source. The initial pressure is one atmosphere and the overall equivalence ratio is .98. The spatial and temporal sizes (Δx,Δt) for most of the calculations are respectively .125cm and 10^{-5} seconds. The spatial step size (Δx) was selected so that the results are relatively insensitive to a further reduction in Δx. The largest permissible Δt for the present computation is controlled by the reaction time scale, which is about 0.1ms for n-octane fuel. It is important to point out that for these step sizes, all four aforementioned numerical schemes produce results, which are indistinguishable from each other; the maximum gas temperature difference between the numerical methods is less than two percent.

The gas temperature profiles are shown in Figure 1. As this Figure indicates, the flame initiation or ignition process is rather slow, taking more than 20ms. However, after this initiation or ignition period, the flame propagates at a much faster rate. It is noteworthy that in the hot region behind the propagating flame, the lowest gas temperature is near the wall. This is due to the nature of the initial temperature profile used for ignition. From these temperature profiles, it seems rather difficult to distinguish between a pre-mixed homogeneous and two-phase heterogeneous cases. This distinction is shown more clearly by the fuel vapor mass fraction profiles, plotted in Figure 2. Because of the slow flame initiation process and rather fast vaporization process for n-octane fuel (with relatively high volatility), a substantial amount of fuel vapor is left behind the propagating flame. This is clearly exhibited by the first peak in the fuel vapor mass fraction profiles. For a relatively less volatile fuel, the vaporization process will be slow and we will not get such a high peak. The same effect could also be obtained by making the flame initiation process faster. It should also be noted that the peak value of Y_f in these profiles continues to increase upto t = 60ms. By that time, the droplets in the hot region are completely vaporized (see Figure 5) and consequently the peak value of Y_f starts decreasing due to diffusion. The second peak, which is more clearly visible at t = 60ms and 80ms, occurs at the propagating flame. The oxidizer mass fraction profiles in Figure 3 portray the propagating nature of the flame more distinctly. Since there is no oxidizer left behind the flame, the amount of fuel vapor in that region remains more or less unchanged. The gas velocity profiles are given in Figure 4. Across the propagating flame region, the gas velocity has the largest value, (110cm/sec) and changes sign. This is also the region where the gas and liquid phase properties have the steepest gradients, and it is due to the resolution of this region that the explicit scheme is superior to the implicit schemes. Corresponding to this maximum velocity, the CFL (Courant-Friedrichs-Lewy) stability condition requires a time step of 1ms, which is the most stringent stability requirement; the diffusion stability limit being Δt larger than 5ms. Since the characteristic time of the chemical process in the present study is about 0.1ms, the time step is completely dictated by this process. This makes the explicit numerical method far superior than any of the implicit methods used here. For example, for the same amount of computation, the computer times for the explicit scheme, iterative implicit without formal linearization, iterative implicit with quasi-linearization, and block implicit with time-linearization respectively, are 8, 32, 33, and 45 minutes. Thus, the explicit method is the most efficient one and the block implicit is the least efficient one. The inversion of block tridiagonal matrix, even by an efficient band matrix solver, is a highly time-consuming process and it makes the block implicit scheme the least favorable.

Figure 5 gives the variation of droplet radius with spatial locations and time. The valleys in these profiles indicate that the gas temperature is the highest in these regions. After t = 60ms, all the droplets in the hot region are completely vaporized. The droplet radius profiles at t = 60 and 80ms indicate an interesting phenomenon at the spatial location, where the profile curvatures change sign. For the calculations presented in Figs. 1-6, a droplet ignition criterion [11] has been used to determine whether there is a flame surrounding individual droplets. To the left of this spatial location, this criterion is satisfied and therefore individual droplets have envelope flames in that region. As a result, the vaporization rate is also relatively high. As we go to the right of this spatial location, the droplet ignition criterion is no longer satisfied, there are no envelope flames, and consequently the vaporization rate and rate of decrease of droplet size reduces. Thus the proper identification of the droplet ignition phenomenon may be very important in spray combustion studies. As shown in Figure 6, the droplet density number increases to the right of the propagating flame because of the droplet velocities, induced by the gas velocity. However, the total number of droplets in the combustor does not change. The droplet velocity profiles are similar to the gas velocity profiles and are not shown here.

Figure 7 shows the effect of changing cold gas temperature on the two-phase flame propagation. A comparison of Figures 1 and 7 indicates that increasing the cold gas temperature from 300°K to 400°K causes a marked increase, not only in the flame initiation process, but also in the flame propagation speed. Furthermore, the gas temperatures in the hot region are higher in Figure 7 than in Figure 1, because the gas pressure increases at a faster rate in the former case.

Figure 8 gives the temperature for the case when there is no envelope flame surrounding any individual droplet. This case is obtained by simply assuming that the droplet ignition criterion is never satisfied and therefore the droplets are only vaporizing. A comparison of these profiles with those when there are individual burning droplets (Figure 7) indicates that flame propagation is faster in the latter case. A simple explanation is that in the regions where droplet ignition criterion is satisfied, the total burning (combusting) rate is much larger than in the non-burning droplet case and this causes an increase in the flame speed.

Another interesting comparison of the burning and non-burning droplet cases is demonstrated in Figure 9, where the droplet radii are plotted versus spatial locations at different instances of time. For the completely non-burning droplet case, the rate of decrease of droplet is smaller than the corresponding case when there are individual burning droplets. This is because the vaporization rate for the burning

droplets is much higher (about twice as high in the present study) than that for the purely vaporizing droplets. Also, the change in curvature of the droplet radius profiles as discussed earlier for the burning droplet case, is not observed when the droplets are purely vaporizing. The conclusions regarding the efficiencies of numerical schemes remain unaltered for the cases: a) when cold gas temperature is raised to 400°K, and b) when droplets are considered to be only vaporizing.

The aforementioned numerical schemes have also been used to compute the homogeneous pre-mixed flame propagation. Again the time-step restrictions are imposed by the chemical reaction rather than by any stability limits. To examine this point further, computations are made for n-octane and propane fuels, which have different chemical kinetics parameters. The temperature profiles for these fuels are given in Figure 10. For n-octane fuel, the same amount of computation for the explicit, iterative implicit without formal linearization, iterative implicit with quasi-linearization, and block implicit schemes requires respectively 5, 25, 25.5 and 36 minutes of computer time. For propane fuel, the superiority of the explicit methods increases. This is because the characteristic reaction time is smaller for propane than for n-octane. As a consequence, the flame initiation as well as flame propagation are faster for propane fuel. In addition, the gas properties have relatively steeper gradients in the flame region and all the implicit schemes take a large number of iterations to compute this region with an acceptable degree of accuracy.

It seems appropriate to compare some of the present results with those presented in an earlier study [6], which considered the flame propagation in air- n-decane fuel droplet mixture with non-uniform droplet interior temperature. The results of that study indicated the existence of a secondary diffusion-like flame behind the primary propagating flame. The secondary flame is not observed in the present calculations. The reason is the highly volatile nature of n-octane, which always creates a fuel rich zone in the vicinity of the propagating flame. For n-decane fuel, which is not so volatile, a fuel lean zone is formed near the propagating flame. This causes some unburnt oxidizer to be left behind the primary flame, which subsequently diffuses towards the initially formed fuel rich zone (near the left end of the combustor) and forms a secondary diffusion flame.

CONCLUSIONS

(1) An unsteady flame propagation in a two-phase heterogeneous mixture is studied by using four different finite-difference schemes; an explicit method, an iterative implicit method without any formal linearization, an iterative implicit method with quasi-linearization, and a time-linearization block implicit method.

(2) The results indicate that the explicit scheme is by far the best. This is mainly due to the fact that the time step size is controlled by the chemical reaction and vaporization rates, and not by any stability requirements.

(3) Amongst the implicit methods, the straightforward implicit scheme without any formal linearization is the most efficient for the present calculations. Thus, a quasi-linearization process does not expedite the convergence of the solutions, at least for the problem considered in the present study. The block implicit scheme is the most expensive one, as the inversion of a block tridiagonal matrix even by an efficient band-matrix solver is a time-consuming process.

(4) Conclusions (2) and (3) should not be accepted in a general sense. Implicit schemes can become attractive if (a) a very high spatial resolution is needed and/or a locally refined mesh is used; the latter situation arises in flows with more than one length scale, as is the case for flows with thin boundary layers, (b) the temporal accuracy is of no importance; for example, in the computation of steady state flows via asymptotic temporal approach, and (c) the fuel used is not so volatile. The block implicit scheme may have an advantage in situations where a large number of iterations in an iterative implicit scheme, is required. Furthermore, the block implicit scheme should be used when the number of PDE's in the block is equal to the number of flow variables to be solved. Such was not the case in the present formulation and consequently, an iteration was required even for the block scheme.

(5) The physical process modeled here is inherently stiff, e.g., the various time scales are quite disparate. In this situation, the use of an operator splitting should be examined. Also, the method of lines should be explored.

(6) Recently, an Eulerian-Lagrangian scheme has been successfully used to solve a two-phase, two-dimensional jet flow [13]. It is recommended to explore the employment of such a scheme for the physical situation presented here.

ACKNOWLEGEMENT: The authors acknowledge the financial support of the Army Research Office for conducting this research.

REFERENCES

[1] Bellman, R.E. and Kalaba, R.E., Quasi-Linearization and Non-Linear Boundary Value Problems, American Elsevier, New York (1965).

[2] Briley, W.R. and McDonald, H., Journal of Computational Physics 24, 372-397 (1977).

[3] Cheng, S.I., "A Critical Review of Numerical Solution of Navier-Strokes Equations," Department of Mechanical and Aerospace Engineering, Report No. 1159, Princeton University, Princeton, New Jersey (February 1974).

[4] Sharma, O.P. and Sirignano, W.A., Combustion Science and Technology 1, 95 (1969).

[5] Lindemuth, I. and Killer, J., Journal of Computational Physics, Vol. 13, p. 181 (October 1973).

[6] Seth, B., Aggarwal, S.K. and Sirignano, W.A. Combustion and Flame 39, p. 149 (1980).

[7] Ranz, W.E. and Marshall, W.R., Chemical Engineering Progress 48 (1952).

[8] Reid, Sherwood, and Prausnitz, The Properties of Gases and Liquids, McGraw-Hill, New York (1977).

[9] Ingebo, R.D., NACA Technical Note 3762 (1962).

[10] Chigier, N.A., Progress in Energy and Combustion Sciences 2, p. 97-114 (1977).

[11] Law, C.K., Combustion and Flame 31, pp. 285-296 (1978).

[12] Raithby, G.D., Computer Methods in Applied Mechanics and Engineering 9, p. 75-103 (1976).

[13] Aggarwal, S.K., Fix, G.J., Lee, D.N., and Sirignano, W.A., Proceedings of the Fourth International Symposium on Computational Methods for Partial Differential Equations, Lehigh University, 1981.

TABLE 1 - SOURCE TERM FOR THE GAS-PHASE EQUATIONS (1-7)

$S_\rho = \dot{m}\, n$

$$\dot{m} = (1 + .3\, R_{e_\ell}^{.5})\, 4\pi\, R_\ell\, \mu\, \ell_n \left[\frac{1-Y_f(1-\delta_f) + \vartheta\, \delta_f\, Y_O}{1-Y_{fs}}\right]$$

$$R_{e_\ell} = 2\, R_\ell\, |u - u_\ell|\, \rho/\mu$$

$S_f = -\dot{w}\, W_f + S_\rho(1-Y_f)$, where

$$\dot{w} = \frac{A\, e^{-E_r/T}\, \rho^2\, Y_O Y_f}{W_O W_f}$$

$S_O = -\dot{w}\, W_O\, M_O - S_\rho Y_O$, where

M_O = 5 for propane
= 12.5 for octane

$$S_\phi = \frac{p^{1-\gamma/\gamma}}{C_p}\left[\dot{w}\, Q - S_\rho\, \{C_p(T-T_\ell) + L'\}\right]$$

$$L' = \frac{(1-Y_{fs})\, [C_p(T-T_\ell) + \vartheta\, \delta_f\, Y_O\, Q/W_f]}{Y_{fs} + \vartheta\, \delta_f\, Y_O - Y_f\, (1-\delta_f)}$$

δ_f = 1 for burning droplets
= 0 for vaporizing droplets

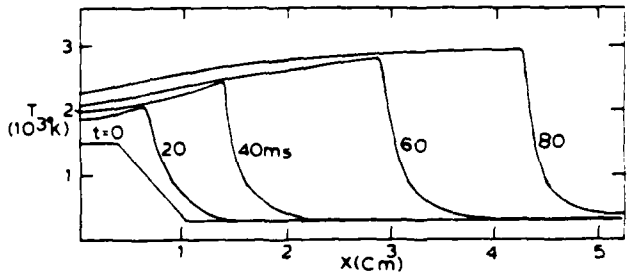

Fig.1 Gas Temperature Profiles for Two-Phase Case

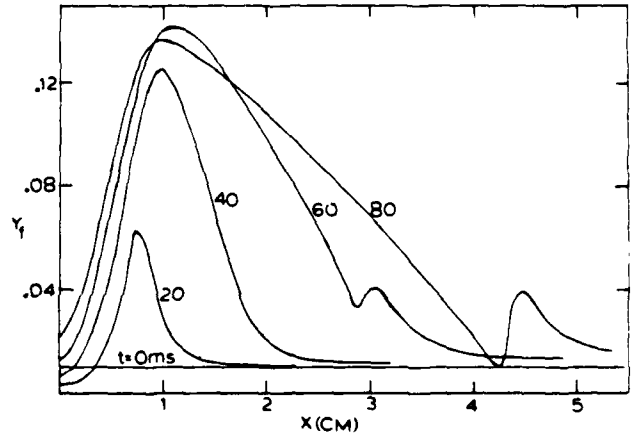

Fig.2 Fuel Vapor Mass Fraction Profiles, Two-Phase Case

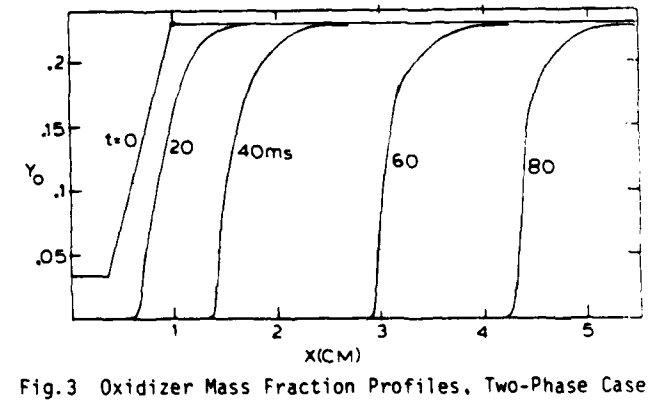

Fig.3 Oxidizer Mass Fraction Profiles, Two-Phase Case

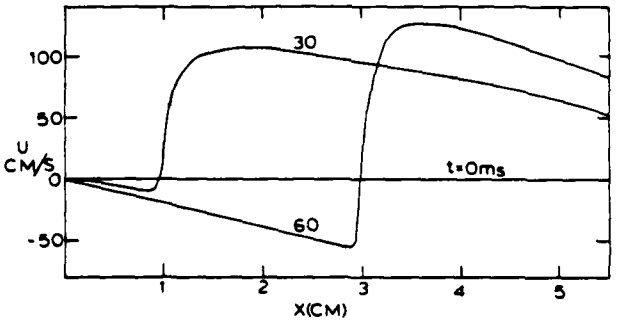

Fig.4 Gas Velocity Profiles, Two-Phase Case

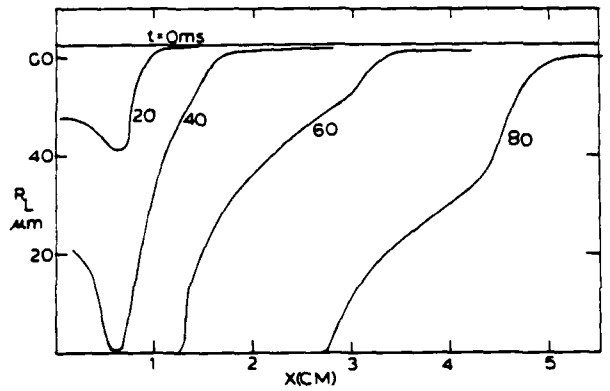

Fig.5 Droplet Radius Profiles

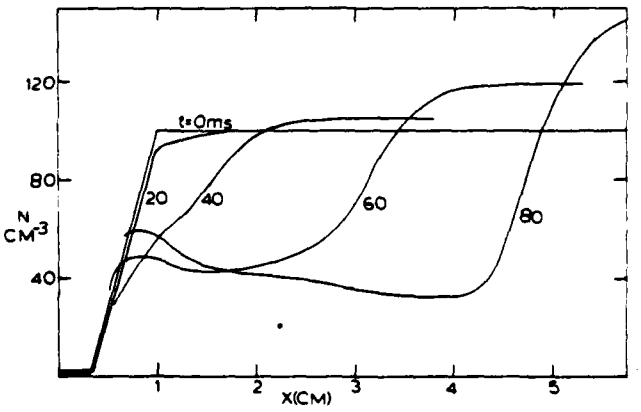

Fig.6 Droplet Number Density Profiles

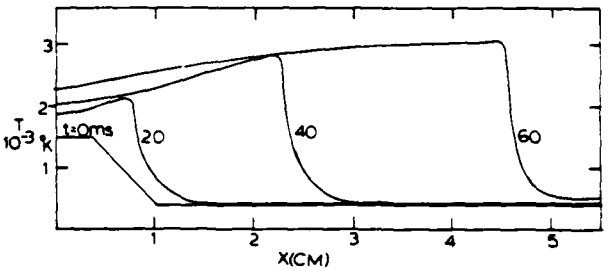

Fig.7 Gas Temperature Profiles, Initial Temperature = 400°K, Two-Phase Case

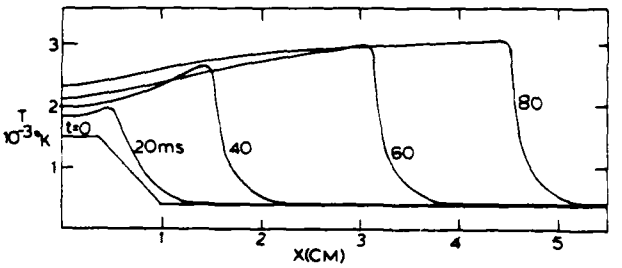

Fig.8 Gas Temperature Profiles (Purely Vaporizing Droplets), Two-Phase Case

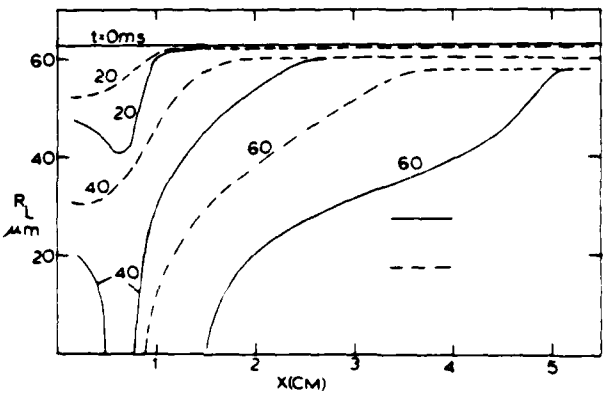

Fig.9 Droplet Radius Profiles, With and Without Droplet Ignition

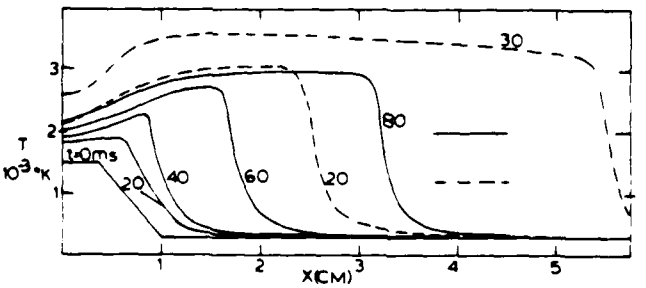

Fig.10 Temperature Profiles for Homogeneous Pre-Mixed Case

DEVELOPMENT OF MULTI-ORIFICE IMPULSED SPRAY GENERATORS FOR HETEROGENEOUS COMBUSTION EXPERIMENTS

by

Nasser Ashgrizzadeh
Graduate Student

and

Shi-Chune Yao
Associate Professor

Department of Mechanical Engineering
Carnegie-Mellon University
Pittsburgh, PA 15213
U.S.A.

ABSTRACT

A multi-orifice impulsed spray generator with two different modes of operation is developed. The impulse jet operation mode covers a wide range of droplet frequencies, and produces arrays of droplets with controllable spacing, but with a wide size spectrum. This ejector also operates in pressurized flow mode. In this mode, optimum disturbance frequency breaks up the liquid jets into uniform size droplets, resulting in a monosized spray. Precise control of fuel flow rate and droplet size is obtained. Preliminary combustion studies demonstrate the applicability of this spray generator for parametric studies.

NOMENCLATURE:

D	=	diameter
f	=	frequency
n	=	number of orifices
u	=	velocity
OD	=	outside diameter
v	=	volume
ρ	=	density
σ	=	surface tension
λ	=	wave length
ϕ	=	air/fuel ratio

SUBSCRIPTS:

d	=	droplet
j	=	jet
l	=	liquid
min	=	minimum
o	=	oxidizer
opt	=	optimum
t	=	tube

INTRODUCTION

Methods to generate a controlled spray have been of major concern to heterogeneous combustion research for years. Such sprays would be very useful in that the effect of important parameters, such as the droplet size and overall fuel-oxidizer ratio, on the combustion could be checked. Different methods have been used to generate a monodisperse spray. Burgoyne and Cohen (1,2) used a spray generator based on the principle of Sinclair-LaMer (3) and LaMer et al. (4) aerosol generator to study the effect of droplet size on the burning velocity in sprays. The monosize spray was obtained by condensation of saturated fuel vapor. The simultaneous control of the droplet size and the amount of condensed fuel is extremely difficult. Therefore, air fuel ratio in Burgoyne and Cohen's experiments was not a constant over the range of droplet sizes studied. Only droplet sizes as large as 50μm can be produced; for larger droplet sizes, this is not an attractive method.

Electrostatic atomization was developed by Vonnegut and Neubaur (5) to produce uniform size droplets with diameter of 1μm or less. Rotating disk spray generator has been used for combustion studies by many researchers (6,7) where the droplet size and number density are

controlled by adjusting the rotating speed of the disk and the fuel feed rate, respectively. The fuel is atomized into droplets in all directions and the control of droplet flow without loss of monodispersity is difficult. Also the work of Friedman et al. (8) indicated that when these sprays are loaded heavily, the uniformity of the spray diminishes.

Vibrating capillary technique which was developed by Dimmock (9,10) (10-300μ drops), Margarvey and Taylor (11) (500μm-20mm), and Mason et al (12,13) (30-1000μ) to produce a stream of monosized droplets, was modified by Dabora (14) to produce a monodispersed spray. He used ten vibrating capillary needles fitted in a plate to produce ten streams of monosize droplets. Many streams are needed to represent a spray.

The impulsed multi-orifice spray generator developed here suits parametric studies of spray combustion. This spray generator can be operated with two different modes. When the fuel chamber is not pressurized, an array of droplets are ejected from the orifices on the plate with each pulse of the piezoelectric transducer. The axial spacing of the droplet streams can be varied directly with the frequency of the pulse, but a spectrum of droplet sizes is produced. The other operating method of the same device is to pressurize the fuel chamber in which droplets with uniform size are produced with the optimum frequencies of Rayleigh jet breakup by the piezoelectric oscillation.

The multi-orifice plate spray generator offers the advantage of flexibility in parametric studies of spray combustion. In this paper we will describe the details of this generator and its operating behavior. Also the design of an apparatus for the combustion study of laminar monodispersed droplet flow with the preliminary combustion results presented.

MULTI-ORIFICE IMPULSED SPRAY GENERATOR

The principle of the multi-orifice impulsed spray generator design is to utilize the pressure pulse from a piezoelectric transducer (Model 104-95NS, Piezoelectric Product Inc.) to control the ejection of the droplets. A large circular piezoelectric transducer is used to pressurize the fuel chamber and to eject the droplets from a plate with many orifices on it.

The generator which has been designed is composed of a body (see Fig. 1) with a multi-orifice plate mounted at the top side and a piezoelectric transducer at the bottom side. The interior of the generator, which is the fuel chamber, is machined smoothly without sharp edges, because sharp corners may induce cavities during pulsation. Since the displacement of the piezoelectric is very small, the existence of a small cavity would absorb the pressure pulse of the piezoelectric transducer.

Since the contraction and expansion of the piezoelectric crystal under electric pulse is very small, bilaminar plate arrangement (15) is used to amplify the displacement. This bilaminar plate is made by epoxying the piezoelectric crystal on a larger brass plate of 4 cm diameter. When the axially polarized piezoelectric plate is exposed to an electric field in the direction of the polarization, there appears an axial expansion and radial contraction of the piezoelectric plate. The axial expansion is small, however, the radial contraction gives a concentric moment that bends the composite plate toward the fuel chamber as an applied pressure impulse.

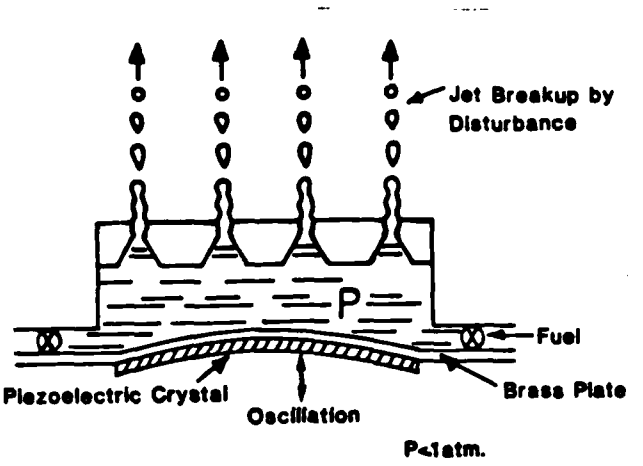

Figure 1 Pressurized flow operation. Uniform size droplet streams are produced.

Two types of operations of this impulsed spray generator can be performed:

Impulse Jet Operation

When the fuel in the chamber is not pressurized, the droplets can be ejected from all the orifices at any applied frequency of the piezoelectric transducer. When a voltage pulse is applied to the piezoelectric plate a pressure pulse is generated in the container. As a result, an array of droplets is ejected. When the pulse ends, the plate returns to its original position and the orifices on the generator are refilled with fuel by capillary effect. Pressure inside the chamber is very close to the atmospheric pressure. The initial design parameters, such as the orifice length and shape, pulse pressure, and pulse duration developed by Beasly (16) for a single orifice was modified for multi-orifice conditions in (17).

It is very important to maintain a minimum thickness of the orifice plate to prevent air bubbles from being sucked into the fuel chamber. This problem usually occurs when the miniscus retreats back into the chamber after the droplet is ejected. A thick plate (1.2 cm) and a thin plate (0.6 mm) have been tested and the thick plate appeared to be the better one in eliminating the air bubble in the chamber. On the other hand, the thicker the plate, the more the viscous force will attenuate the pressure pulse. This problem can be overcome by making the orifice diameter varying as a converging nozzle viewing from the fuel chamber.

An optimal distance between the piezoelectric plate to the orifice plate is required. The constraint on the piezoelectric operation is the maximum applied voltage. Therefore maximum pressure and displacement also occur for each piezoelectric plate. In order to offer the required magnitude of the pressure pulse to the orifices, a short distance between the piezoelectric plate and the multi-orifice plate is desirable. However, very short distance would generate an array of droplets with non-uniform sizes. The droplets near the center of the plate would be ejected faster due to the uneven buckling of the piezoelectric plate.

In this type of operation, the droplet generation

frequency can be varied as desired. However, the generated droplets usually show a wide spectrum of sizes. This is because the orifices at different positions on the plate will experience different magnitudes of pressure pulses. In practice, if there exists a liquid film on the top of the orifice plate, the generated droplet will have to tear away from the liquid film and will have a different size from that generated from a hole on a dry plate. This liquid film exists usually due to the minor leakage of liquid from the slight pressure differences across the orifice plate. Additionally any imperfections of the orifice hole will cause the disturbance of the pressure wave in the hole and the generation of satellite droplets during the injection.

Pressurized Flow Operation

The other type of operation of the same device is to pressurize the fuel chamber so that liquid jets flow continuously. With a specific pulse frequency applied at a jet velocity, the liquid jet breaks up into uniform size droplets (Fig. 1.). The phenomenon of uniform liquid jet break-up was first observed experimentally by Savart (18) and studied theoretically by Plateau (19) and Rayleigh (20,21). From the consideration of surface energy, Plateau derived the minimum wavelength λ (distance between unstable disturbance) on an infinitely long liquid cylinder.

$$\lambda_{min} = \pi D_j \tag{1}$$

where D_j is the liquid jet diameter. For an inviscid, incompressible, cylindrical liquid jet sprayed into a vacuum Rayleigh derived the optimum wavelength for a most unstable disturbance.

$$\lambda_{opt} = 4.508\ D_j \tag{2}$$

Schneider and Hendricks (22) experimentally determined that uniform droplets could be produced by varying λ within the following range:

$$3.5\ D_j < \lambda < 7\ D_j \tag{3}$$

Weber (23) extended the analysis to include the effects of the liquid viscosity and the velocity of the jet, but Crane et al (24) showed that if the velocity is low (less than 10 $^{m}/_{s}$) these effects can be neglected. Considering the conservation of energy Lindblad and Schneider (25) derived a minimum liquid velocity needed to form a liquid jet from a capillary tube.

$$u_j = \left(\frac{8\sigma}{\rho D_j}\right)^{1/2} \tag{4}$$

where σ is the surface tension and ρ is the density of the liquid. Dabora (14) experimentally showed that actual minimum velocities are lower by 25-35% than this relation indicated.

The diameter of the liquid droplet particles from the impulsed orifice generator can be calculated from jet velocity and the disturbance frequency using simple mass conservation equation. That is

$$D_d = \left[\frac{3}{2} D_j^2\, u_j/f\right]^{1/3}. \tag{5}$$

This kind of operation is very similar to that of the Berglund & Liu Aerosol Generator (26); however, the present device generates droplets from many orifices so that a spray with very dense droplets and little turbulence is produced. The number of active orifices on the plate can also be varied by plugging the orifices or by using a different plate with different numbers and patterns of orifices. Therefore, to generate a spray with a fixed droplet size from a given orifice plate the u_j/f is changed (see equation (5)) to give different fuel flow rates. When the operation beyond the limits of equation (3) is desired, the plate is substituted with another plate with different orifices.

The number of operating orifices can be related to the air/fuel ratio, ϕ for any particular droplet size and air flow velocity from the consideration of mass conservation.

$$n = \frac{3}{2}\frac{D_t^2}{D_d^3}\frac{u_o}{f} \cdot \frac{\rho_o}{\phi \rho_f^* \rho_o} \tag{6}$$

As an example, for a stoichimetric hexane air mixture with 2 m/s air velocity and droplet of 285μm at 3000HZ, 12 orifices are needed on a plate with 5 cm diameter.

COMBUSTION FACILITY

In order to study the combustion behavior of a spray generated by the present device, a special experimental set up is fabricated as shown in Figure 2. Generated droplets flow vertically upward through several pieces of tubes which have a diameter of 9 cm and length of 4 cm each. A uniform suction at the downstream moves the droplet flow vertically upward. Air is sucked from the quiescent atmosphere through the spacings of the tubes. As a result, the droplets will not collide with the wall.

Air is also ejected into the droplet flow through an array of tubes situated in between the rows of the orifices on the plate. The air tubes are 0.31 cm OD with aligned holes drilled on them. The hole positions are adjusted to give uniform flow, the pressurized air flow is metered before fed into the tubes. With the air jet flow, the stream of droplets may be slightly dispersed to prevent coalescence of the droplets.

The spray is ignited with a hydrogen pilot flame. Very small amounts of hydrogen flow is ejected from the fine holes on the top side of a horizontal tube of 1.6 mm O.D. After ignition, the hydrogen flow can be terminated then the tube also acts as a flame holder. A steady V shaped spray flame can be sustained on this tube. Knowing the gas and liquid flow velocities, and the stream lines flame speed can be estimated from the angle of the V flame.

RESULTS AND DISCUSSION

The characteristics of the multi-orifice impulsed spray generator are studied for two different multi-orifice plates. In making the 60μm orifice plate, a special carbide drill has been used. Table (1) indicates the dimension and the number of orifices as well as the material of each plate. The estimated size variations of the orifice is within 5 μm. Also the ranges of the monosize droplets at pressurized flow operation are also indicated in the Table.

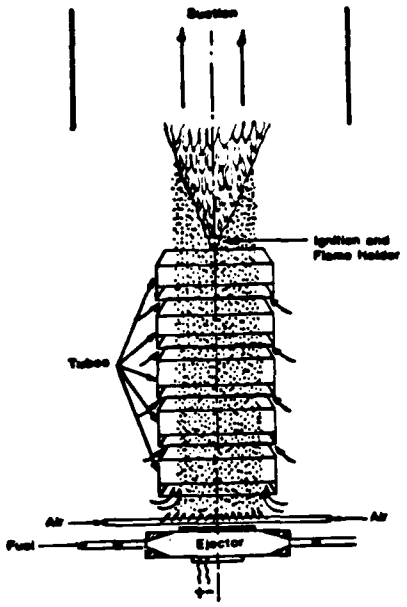

Figure 2 Overall Setup for the Combustion Studies.

Table 1

Multiorifice Plate	#1	#2
Orifice Diameter:		
Exit	60 μm	150 μm
Inlet	0.6 mm	2 mm
Number of Orifices	221	39
Orifice Spacing	3x3	4x10
Plate Thickness	0.6 mm	1.2 cm
Material	Stainless steel	Brass
Orifice Nozzle Shape	Connical	Stepwise Cylinders
Plate Diameter	6.9 cm	6.9 cm
Droplet Diam. Range Obtainable	104-131	260-330

Figure 3 shows the spectrum of droplet size as the percent of volume for 150μm orifice plate under impulsed jet operating conditions. A microscope with magnification up to 112 times is used for the photographing of the droplet sizes. The strobe light is triggered by the shutter of a Polaroid camera which is attached to the microscope. Droplet size spectrum in Figure 3 is found from the measurement over 1000 droplets from photographs that were magnified 14 times. Although a wide spectrum is observed, it is clear that there is a peak between 220 to 300μm. The smaller peak near 150μm is possibly originated from the satellite droplets. The spray generated at this operation condition is suitable for studying poly-dispersed spray combustion with the droplet spacing adjustable arbitrarily.

Figure 4 shows the size spectrums of the droplets at pressurized flow operating condition for 150μm orifice plate at two different flows and frequencies. Monosize droplet spray with about ± 10μm deviation from the mean droplet size can be obtained, Fig. (4-B). This deviation is possibly because the orifices are not exactly the same in size. Also the u_j is possibly slightly different for the orifices at the sides and at the middle of the plate. This is observed by the maximum height droplets reach when ejected vertically up under stagnant ambient. It is seen that the maximum height reached by droplets ejected from side orifices is slightly smaller than the ones in the center of the plate. Larger size droplets will be produced near the middle of the plate if the averaged pressure is higher there. The spectrum in Figure 4 is obtained by photography measurement. The typical pricute of the droplet streams taken close to the plate is shown in Figure 5.

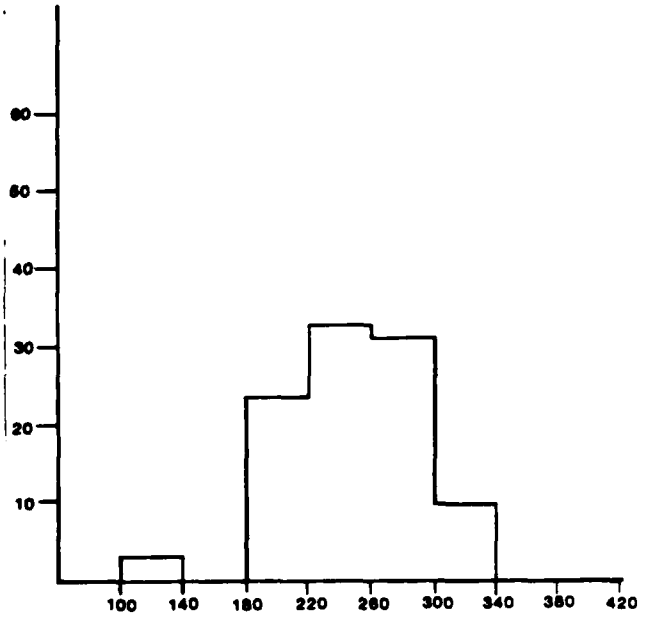

Figure 3 Droplet size spectrum by photography measurement technique, for impulse jet ejection operation at 1000HZ frequency.

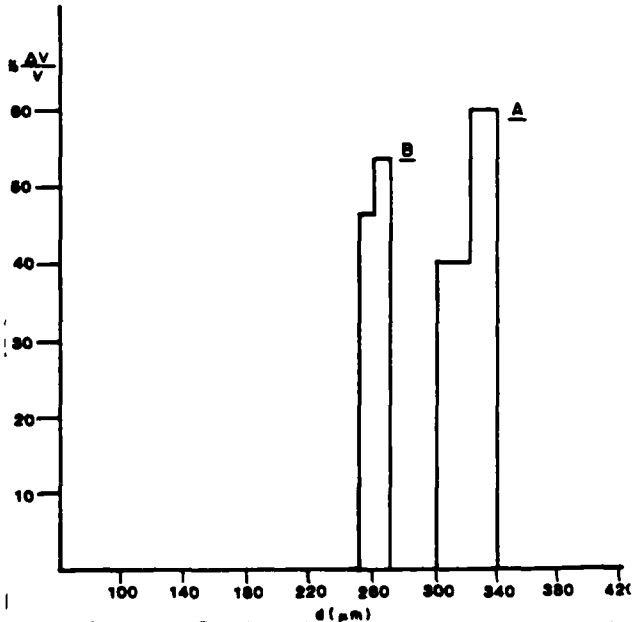

Figure 4 Droplet size spectrum by photography measurement technique for pressurized flow operation. (A. 3700HZ and 40cc/min, B. at 2800HZ and 40cc/min Hexane Flow Rate.)

When spray is generated at pressurized flow condition, the required fuel flow rate and the impulse frequency to give a desired droplet size can be evaluated prior to the experiment with good accuracy. Figure 6 shows the operating range of the 150μm multi-orifice plate. The obtainable range of droplet size is between 260μm and 330μm. This can be evaluated from equations (3) and (5) assuming $\lambda = u/f$ where the λ is variable in a range as described in equation (3). The curves of droplet size versus frequency are drawn using equation (5) with three different jet velocities of 2.1, 2.6 and 3.3 $^{m}/_{s}$ as the solid line in Figure (6). These jet velocities are evaluated from the measured mass flow of fuel through the generator. The hexane flow rate can be set to produce the required jet velocity. Then droplet sizes at different frequencies are obtainable. The agreement between the experimental points and the curves predicted from equation (5) is reasonable.

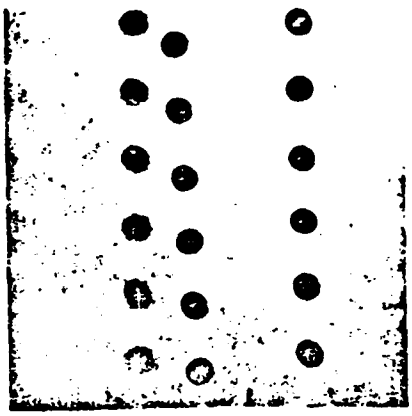

Figure 5 Streams of uniform size droplets near the orifice plate.

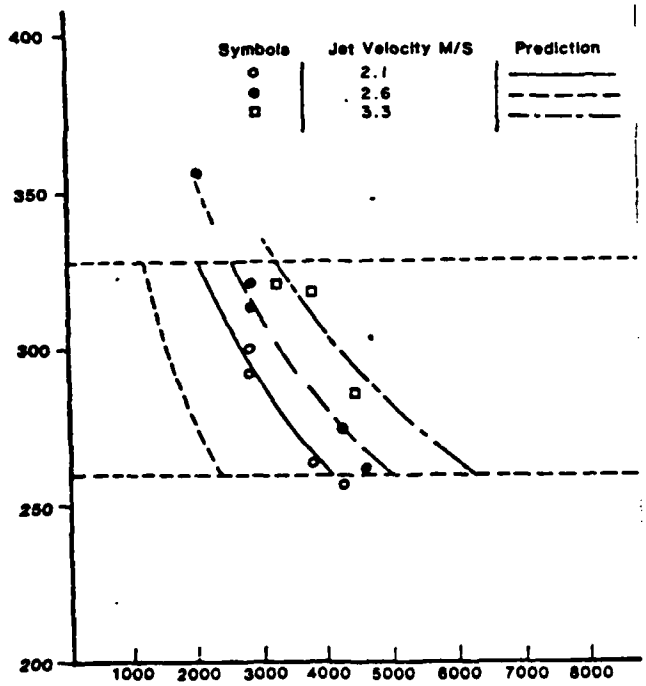

Figure 6 Operation range for the 150μm orifice size plate.

In order to demonstrate the combustion, a monosize spray of 285μm mean droplet diameter generated at 3000 HZ frequency, 2.1 $^{m}/_{s}$ jet velocity from 19 operating orifices is considered. Air tubes are adjusted to give a steady upward homogeneous flow of droplets at the ignition point. Gas velocity profiles are measured separately under cold condition with no droplet flow using a hot film anemometer.

Pictures of the spray are taken near the ignition point using strobe light and the microscope. Examining the photographs, it is noticed that the spray has always kept its monosize distribution. Pictures of the sustained V-shaped flame on the horizontal flame holder are shown in Figure 7(a). Figure 7(a) shows the flame of isohexane spray with initial droplet size of about 285 μm. By studying this steady flame, detailed behavior of the flame propagation in the vicinity of the flame front can be observed with the microscope. A spark source (strobe light) with 3 μs duration is used to illuminate droplets. Figure 7(b) shows the flame of isohexane spray with initial droplet size of 150 $\pm$ 10 μm. It is shown that all droplets vaporize completely ahead of the flame and a blue flame is obtained And Figure 7(c) shows the flame of Toluene spray with initial droplet size of 285 μm. No blue flame is observed.

Through various combustion studies, it is observed that the large droplets of 285μm would not completely vaporize in the preheat zone. When the droplet number density is low, individual droplets burn in blue envelope flames. As the number density is increased, the flame shape and structure changes to a yellow flame with a rough flame front. The details of the combustion results will be presented in a future paper.

Figure 7a Steady isohexane spray flame with initial droplet size of 285 μm using a 3 μsec spark source. Spark light shows droplets approaching the flame front.

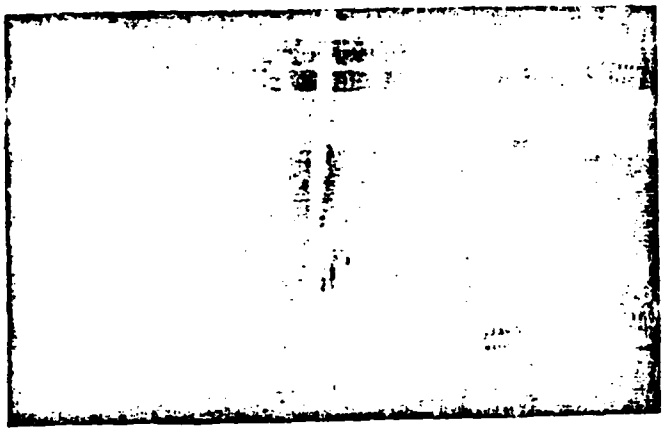

Figure 7b Isohexane spray flame, with initial droplet size of 130 μm. The blue flame shows all the droplets are vaporized ahead of the flame.

Figure 7c Toluene spray flame with initial droplet size of 285 μm. No blue flame. Flame front is not smooth.

CONCLUSION

A multi-orifice impulsed spray generator with two different modes of operation was developed. The impulse jet operation mode covers a wide range of droplet frequency and produces arrays of droplets with controllable spacing, but with a wide size spectrum. Pressurized flow operation applies disturbance frequency to break up the liquid jets into uniform size droplets, resulting in a monosized spray. Precise control of fuel flow rate and droplet size is obtained. Preliminary combustion studies demonstrated the applicability of this spray generator for parametric studies.

REFERENCES

1. Burgoyne, J.H. and Cohen, L., "Effect of Drop Size on Flame Propagation in Liquid Aerosols." Proc. Roy. Soc., 1954, Vol. A225, No. 1162, pp. 375-392.

2. Burgoyne, J.H. and Cohen, L., "Production of Monodispersed Aerosols of Large Drops," J. Colloid Sci., 1953, 8(3), p. 364.

3. Sinclair, D. LaMer, V.K., "Light Scattering as a Measurement of Particle size in Aerosols," Chem. Rev., 1949, 44, p. 245.

4. LaMer, V.K., Inn, E.C.Y. and Wilson, I.B., "The Method of Forming, Detecting and Measuring the Size and Concentration of Liquid Aerosols in the Size Range 0.01-0.25 Microns Diameter," J. Colloid Sci., 1950, 5, pp. 471-497.

5. Vonnegut, B. and Neubaur, R., "Production of Monodispersed Liquid Particles by Electral Atomization," J. Colloid Sci., 1952, 7(6), p. 616.

6. Hayashi, S., Obtani, T., Iinuma, K., and Kumagai, S., "Limiting Factors of Flame Propagation in Low-Volatility Fuel Clouds," Eighteenth Symposium (Int.) on Combustion, The Combustion Institute 1981, pp. 361-367.

7. Bolt, J.A. and Boyle, T.A., "The Combustion of Liquid Fuel Spray," Trans. ASME 78, (1956), 609.

8. Friedman, S.J., Gluckert, F.A. and Marshall, W.R., Jr., Chemical Engineering Progress, Vol. 48, April, 1952, pp. 181-191.

9. Dimmock, N.A., "Production of Uniform Droplets," Nature (Engl), 1950, Vol. 166 pp. 586-687.

10. Dimmock, N.A., "The Controlled Production of Streams of Identical Droplets," Nat. Gas Tub. Est. (Engl), Memo M 115, 1961.

11. Magarvey, R.H. and Taylor, B.W., "Apparatus for the Production of Large Water Drops," The Rev. of Sci. Inst., Nov. 1956, Vol. 27, No. 11, pp. 944-47.

12. Mason, B.J., Jayoratne, P.W., and Woods, J.D., "An Improved Vibrating Capillary Device for Producing Uniform Water Droplets of 15 to 500 μm Radius," J. Sci. Inst., 1963, Vol. 40, pp. 247-49.

13. Mason, B.J. and Brownscombe, J.L., "Production of Uniform Size Drops at Controllable Frequency and Spacing from a Vibrating Capillary," J. Sci. Inst., May 1964, Vol. 41, pp. 258-259.

14. Dabora, E.K., "Production of Monodispersed Sprays," The Review of Scientific Instruments, Vol. 38, No. 4, 1967.

15. Ashton, J.E. and Whitney J.M., "Theory of Laminated Plates," Stanford, Conn.: Technomic, 1970, pp. 1-29.

16. Beasly, J.D., "Model for Fluid Ejection and Refill in Air Impulse Drive Jet," Photographic Science and Eng., Vol. 21, No. 2 (March/April, 1977).

17. Ashgrizzadeh, N., Yao, S.C. and Sirignano, W.A., "Progress on Impulse Jet Droplet Generator for Laminar Spray Combustion Experiments," Eastern Section/Combustion Institute, Princeton, New Jersey, p. 44, (1980).

18. Savart, Ann. Chimie 53, 337 (1833).

19. Plateau, "Statique Experimentale et Tehorique des Liquids saumis aux seules Forces Moleculaires," (1873) Ref. in "Theory of Sound," by J.W.S. Rayleigh, 2nd ed., Vol. 11, 363 (1878), Reprinted by Dover Publi., N.Y. 1945.

20. Rayleigh, Lord, Proc. Roy. Soc. 29, 71, (1879).

21. Rayleigh, Lord, Proc. London Math. Soc., 10.4, (1878).

22. Schneider, J.M., Hendricks, C.D., Rev. Sci. Instrum. 35 (10), 1349-50 (1964).

23. Weber, C., Z. Angew., Math and Mech. 11, 136, (1931).

24. Crane, L., Birch, S. and McCormack, P.D., Brit. J. Appl. Phys. 15, 743, (1964).

25. Lindblad, N.R. and Schneider, J.M., "Production of Uniform-sized Liquid Droplets," J. Sci. Instr. 42, 635, (1965).

26. Berglund, R.N. and Liu, Y.H., Environmental Sci. & Tech., Vol. 7, pp. 107-153, (1973).

EFFECT OF THERMAL RADIATION ON THE DROPLET PRE-EVAPORATION IN SPRAY COMBUSTION

Shi-chune Yao
Associate Professor

Nassar Ashgrizzadeh
Graduate Student

Department of Mechanical Engineering
Carnegie-Mellon University
Pittsburgh, PA 15213

INTRODUCTION

In many combustion systems the flame and the combustion products are at very high temperatures such that thermal radiation plays a significant role in the transport of combustion heat [1]. Generally, the combustion process of gases is not strongly influenced by the thermal radiation from the hot zone because the absorptivities of gases are usually small. However, the combustion process of two phase mixtures could be affected by radiation significantly because of the high absorptivities of the participating liquid or solid phases.

Different from heat convection, thermal radiation is a far-field interaction. In spray combustion the droplets could be heated up and possibly evaporated by the radiation at the far upstream of the flame. Before the spray reaches the flame, the droplet size diminishes, the droplet number density reduces, and the fuel-vapor to air ratio increases as compared with the equivalent case where radiation does not exist. Therefore, the subsequent combustion of the spray is greatly affected because the thermal radiation changes the initial condition of the spray combustion. In extreme cases, the droplets may be pre-evaporated completely and the combustion of the spray becomes a combustion of pre-mixed gases.

The objective of this paper is to study the radiative effect on the droplet flow combustion to reveal the fundamental behavior of this interaction. The radiative transport will be calculated for an idealized one dimensional droplet flow. The transfer number B of droplet considering the thermal radiation is calculated. Finally, calculation is performed for a sample case to demonstrate quantitatively the radiative effect on droplet pre-evaporation.

MODEL

In order to demonstrate the basic principle of radiative transport, a simple model of one-dimensional droplet flow combustion system is considered with its schematic shown in Figure 1.

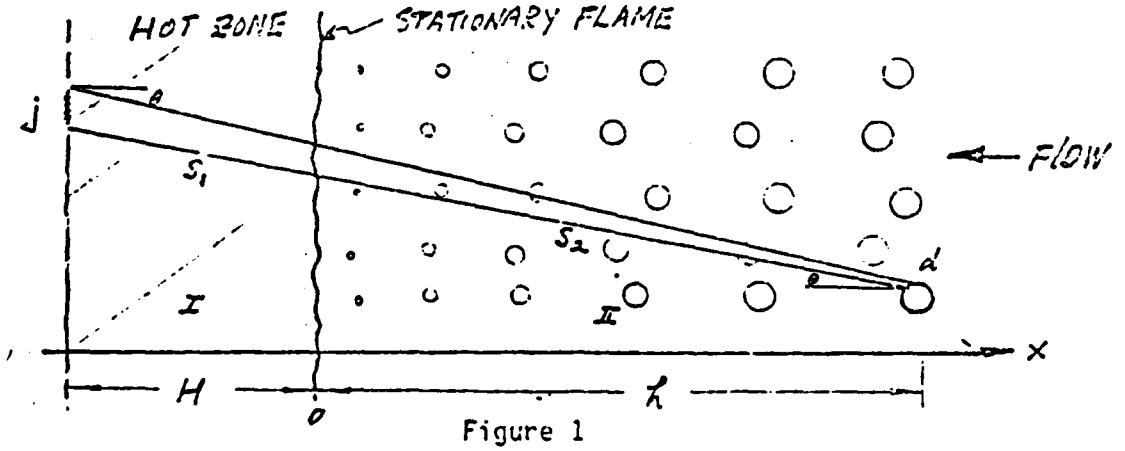

Figure 1

With a stationary flame in space, the combustion products constitute a hot zone with a finite depth and at uniform temperature. Monodisperse droplets are suspended at the far upstream. Due to radiative evaporation the droplet diameter d becomes a function of space x. The hot gases perform as radiation source with self absorption while the droplets at upstream of flame perform as radiative sink.

III. RADIATIVE TRANSPORT

It is intended to find the radiative heat flux to a droplet of diameter d at a distance h upstream of the flame. The droplet is spherical; therefore, the radiation from any angle will see it as a round disk with an area $\pi d^2/4$. The total radiative heat flux $q_{\lambda d}$ for the wave length λ from all the differential areas j to the droplet is

$$A_d q_{\lambda,d} = \sum_j e_{\lambda bg} d\lambda A_j F_{jd} \overline{(\alpha_1 \tau_2)}_{jd} \qquad (1)$$

where $e_{\lambda bg}$ is the black body hemispherical emissive power and $(\alpha_1 \tau_2)_{jd}$ is the geometric mean value of the emittance in hot region and transmittance in the droplet flow region from differential area j to droplet d. Considering the integration of all the symmetric rings of surface element j the equation (1) gives the incident heat flux to the droplet at the wavelength λ

$$q_{\lambda,d} = e_{\lambda bg} d\lambda \int_{A_j} \frac{(1-e^{-a_{\lambda_1} S_1}) e^{-a_{\lambda_2} S_2} \cos\theta}{\pi (S_1+S_2)^2} dA_j \qquad (2)$$

For an one-dimensional system the θ varies from 0 to $\frac{\pi}{2}$. Integrating the equation (2) it becomes

$$q_{\lambda,d} = 2 \left[E_2(a_{\lambda_2} h) - E_2(a_{\lambda_1} H + a_{\lambda_2} h) \right] e_{\lambda bg} d\lambda \qquad (3)$$

where the E_2 is the second exponential integral function.

Not all the radiation incident to the droplet is absorbed by the droplet. Only a fraction, which equals the absorption efficiency, will be absorbed. In the above analysis it has been assumed that forward scattering occurs to the droplets and the radiation property of the two phase mixture is optically thin. For simplicity, it is also assumed that the droplets burn instantaneously when they go into the flame and the burning droplets in the hot region do not participate in radiative energy transport.

In many practical conditions the above assumptions are satisfied. For dielectric fuel droplets with diameter larger than 5μm the radiation from hot gas at a temperature higher than 1500 K will have predominantly forward scattering. The optically thin approximation requires that the photon mean free path is much larger than the characteristic dimension of the system. For droplets with 100μm diameter and 2mm interspacing the radiation properties can be considered optically thin with respect to a characteristic dimension less than 1m.[2].

IV. TRANSFER NUMBER FOR RADIATIVE EVAPORATING DROPLET

The classical transfer numbers of evaporating or combusting droplet have been well established for conductive or convective heat transfer conditions. However, these transfer numbers should be revised for cases where radiation is significant.

Since the gas phase does not participate actively in the radiative transfer, the transfer number of a droplet can be rederived by simply changing the boundary condition of the vapor energy equation. [3]

By performing integration, the transfer number considering radiative effects becomes

$$B_r = \frac{C_p (T_\infty - T_s)}{L - q_d / (4 \rho_v v_v)_{r_s}} \qquad (4)$$

where $V_v/_{rs}$ is the vapor velocity at the droplet surface which can be derived from species equation

$$v_v|_{r_s} = D_s \ln (1 + B_M) / r_s \qquad (5)$$

where the form of B_M is not changed due to radiative. It is interesting to point out that the transfer number B_T is therefore indirectly dependent upon the droplet diameter r_s. As a result, the diminishing of droplet size will no longer follow the d^2 rule exactly.

AUXILLIARY EQUATIONS AND SAMPLE CALCULATIONS

The change of droplet size due to radiative pre-evaporation can be calculated when the β value is known. The β will be evaluated from the B value which is, in turn, dependent upon the radiative heat flux from the hot zone. In general, the radiative flux is a function of x and the size-and-distribution of droplets between the location x and the flame front. Conservation equations can be written for the evaluation of this information without substantial difficulty; however, the calculation will be performed numerically.

In spite of the practical complications of the auxilliary equations, sample hand calculation can be performed to reveal the essential feature of this problem with some approximations. For example, the radiative transport can be calculated easily if a gray system is assumed. For optically thin two-phase-mixture the local heat flux will not be sensitive to the variations of droplet size and distribution in the space. Therefore the d and n can be fixed as constants in the approximated method of solution.

Typical calculations have been performed for stoichiometric mixture of Octane with droplet size 100μm at 1atm. The flame speed is assumed to be 40cm/sec and the length H of the hot zone is selected as 30cm. The calculated transfer number is about 9.6 instead of 5.0 which is the typical value when combustion without radiation The transfer number is found to be sensitive to the thickness and temperature of the hot zone where radiation origin from. As a result, a droplet at 6cm upstream of flame may diminish from 100μm to 75μm in a traveling distance much less than half cm. Of course at other cases of lower flame temperatures the corresponding distance could be longer.

NOMENCLATURE

$a_{\pi 1}$	absorption coefficient of the combustion product at hot zone
$a_{\pi 2}$	absorption coefficient of the two phase mixture
B_T	transfer number due to thermal effect
B_M	transfer number due to mass transfer effect
d	droplet diameter
h	location of droplet, see Fig. 1
H	thickness of hot zone, see Fig. 1
L	latent heat of evaporation of fuel
q_d	radiation heat flux to the droplet, all the wavelength
r_s	instantaneous droplet radius
β	evaporation parameter in the equation for d^2 rate

ACKNOWLEDGEMENT

Valuable discussions with Professor W. Sirignano is greatly appreciated. The second author was supported financially by U. S. Army Research Office during the period of this research.

REFERENCES

1. I. Glassman, COMBUSTION, Academic Press, 1977
2. R. Siegel and J. Howell, THERMAL RADIATION HEAT TRANSFER, McGraw Hill, 1972
3. S. Fineman, MS.E Thesis, Department of Aero. Engineering, Princeton University, 1962

RADIATION EFFECT ON DROPLET PRE-EVAPORATION IN THE CYLINDERICAL COMBUSTION CHAMBERS

Nasser Ashgrizzadeh, Shi-chune Yao

Department of Mechanical Engineering
Carnegie-Mellon University
Pittsburgh, PA 15213

1. Introduction

Radiation effect on the droplet pre-evaporation in spray combustion has recently become a subject of concern, as the theoretical models for droplet spray combustion beeing developed in a more detailed fasion. Radiation effect on evaporation of a single droplet and droplet sprays has usually been neglected, because of its small influence in droplet evaporation. But most experiments in this area were done on protype laboratory scaled systems. Where small scale combustion systems were being studied. So analytical results without consideration of radiation are close to experimental data. Although radiation is a dominant heat source in large scale practical systems and should be included in the analytical models.

In this paper the authors have followed their previous work in Droplet pre-evaporation due to radiation[1]. Previously a model of infinitly long flame was considered for its simplisity of radiation calculations. In this paper a more practical model of cylinderical combustion chamber is considered. Also wall effects which was neglected in the previous work, is included in present paper. Spaldings approach of evaporation of a single fuel droplet in a nonconvective atmosphere of a given temperature and pressure, which was used in previous paper[2], is substituted with a better model of spacially uniform but temporally varying droplet temperature developed by Law[3].

2. Droplet Evaporation In A Radiative Environment

By assuming Fick's Law, Fourier's Law and unitary Lewis-Semenov number we can solve for droplet evaporation[3,4]. A model of spacially uniform but temporally varying droplet temperature in a non-convective environment is solved. Radiation heat is assumed to be the only heat source, to show only the radiation effect on the droplet evaporation. For a typical n-Decane fuel droplet of 100μm diameter, in a non-convective surrounding the assumption of uniform droplet temperature is good as the droplet life time{O(10)msec} is much larger than droplet heat up time{O(10^{-1})msec}. Also for simplicity we assumed all the radiation heat deposites at the surface of the droplet. This assumption can be removed at the expense of incurring additional complexity of absorption of radiation heat at different depths within the droplets[5-7]. The governing equations of a evaporating droplet with above assumptions, is

well established, neglecting the radiation heat[3]. So considering radiation, modification of the analysis would be only at the boundry condition of the droplet. A heat balance at the droplet surface is:

$$k\left(\frac{dT}{dr}\right)_s = m_s L_v + \frac{1}{3} r_s \rho_l C_l \left(\frac{dT}{dt}\right)_s - q_R \qquad (1)$$

A new transfer number is defined as follow:

$$B'_T = \frac{C_p(T - T_s)}{L_v - (q_R - q_h)/m} \qquad (2)$$

where q_h is defined as: $q_h = \frac{1}{3}(r_s \rho_l C_l)(dT/dt)_s$ is the heat required to raise the droplet temperature.

The evaporation rate m can also be found from species equation as:

$$m = \frac{\rho_s D_s}{r_s} \ln(1+B_M) \qquad (3)$$

Numerical calculations for B values show that B in despite of what was thought previously, never blows up. As $[L_v - (q_R - q_h)/m]$ does not go to zero for all practical values of q_R. This can be explained by the direct relation between radiative heat and vaporization rate. So the more radiation the higher the vaporization rate m . So B value defined as above can still be a valuable parameter in problems including radiation heat transfer.

3. Radiation Heat Transfer

In order to find radiative heat, we assume forward scattering to the droplets and the radiation property of the two phase mixture is optically thin. For simplicity it is also assumed that the droplets burn instantenously when they go into the flame and the burnning droplets in the hot region do not participate in the radiative energy transport. A better explanation for these assumption is given by Yao and Ashgrizzadeh[1] . The radiation comming from Hot burning gas region with considering the wall effect of that region, to a droplet located in the centerline of the cylinderical chamber is given by[8]:

$$dQ_{\lambda i,k} = A_k dq_{\lambda i,k} = \sum (dq_{\lambda o,j} A_j F_{j-k} \tau_{\lambda,j-k(1)} + e_{g(1)bg} d_\lambda A_j F_{j-k} \alpha_{\lambda j-k(1)}) \tau_{\lambda,j-k(2)} \qquad (4)$$

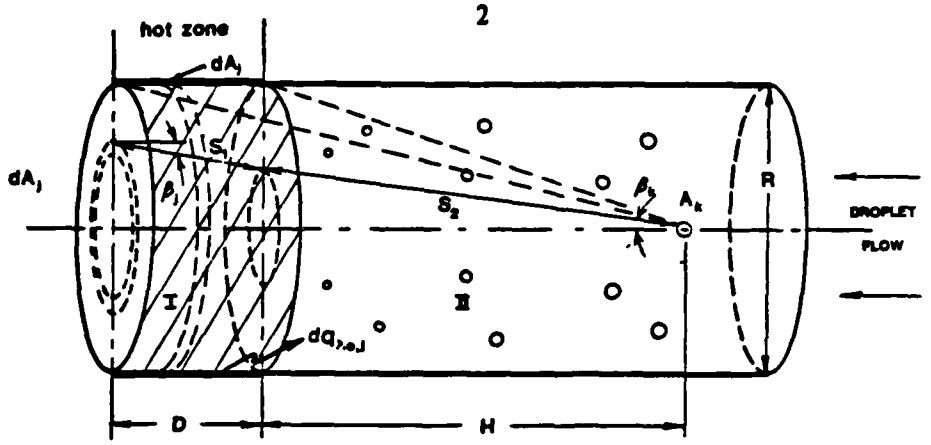

Where $dq_{\lambda_{oj}} = \epsilon_w \sigma_w T^4$ is the radiation from the wall. And the second part of the right hand side is radiation due to the hot gasses. Both terms are attenuated by the factor while passing through cold zone due to existance of absorbing droplets in the radiation path.

$$F_{j-k} = (Cos\beta_j Cos\beta_k)/\pi(S_1+S_2)^2 \tag{5}$$

is the view factor. As droplets are spherical, the radiation from any angle will see it as a round disk with an area $\pi d^2/4$ and $\beta_k = 0.0$. Also:

$$\tau_{\lambda,j-k(1)} = 1- exp(-a_{\lambda_1} S_1) \tag{6}$$

$$\tau_{\lambda,j-k(2)} = 1- exp(-a_{\lambda_2} S_2) \tag{7}$$

$$\tau_{\lambda,j-k(1)} = 1- exp(-a_{\lambda_1} S_1) \tag{8}$$

Integration of equation(1), using equations(2-4) results in the following equation for radiation arriving to a droplet located at a distance h from the flame.

$$dq_{\lambda_{j-k}} = 2\sigma T^4 \{ E_2(a_{\lambda_2} h) - E_2(a_{\lambda_1} D + a_{\lambda_2} h) + E_2[(a_{\lambda_1} D + a_{\lambda_2} h)n] - E_2(a_{\lambda_2} \sqrt{h^2+R^2} - (1-\epsilon_w) \int_{nh}^{\sqrt{R^2+h^2}} exp(-k_{\lambda_1}(h/S_2) dS_2 \} \tag{9}$$

where: $$n = 1 + \frac{R^2}{(h^2+D^2)}$$

and radiation from the wall is assumed to be:

$$dq_{\lambda_{oj}} = \epsilon_w \sigma_w T_w \tag{10}$$

The integration limits were from $S_2 = h$ to $S_2 = \sqrt{h^2 + R^2}$. The last part of equation(5) is

integrated numerically using simpson's rule. Also it was noticed that radiation from the walls are very important, and if combustor has long wall a greate proportion of radiation heat is supplied by the wall. Fig 2 shows the radiation flux to droplets with diameter of 100μm moving toward the flame from a distance of 0.5ft with a velocity of 14ft/sec. Curves are drawn for different geometric sizes of cylinder.

4. Results And Conclusions

Knowing B the droplet vaporization rate can be found by: $\beta=(8/\rho_l)(\lambda/c_p)/n(1+B)$ The results are shown in Fig 1 & 2. An interesting feature noticed by the curves in Fig 2. When the droplet temperature after reaching a maximum value, starts to decrease as droplet gets closer to the radiation source. This is not noticed in the pre-evaporation zone of systems of relatively low radiative heat, Because droplet heat up progresses very slowly relatve to the residence time in cold zone. If a very long cold region or a long residence time is taken, the same feature namely the reduction of droplet temperature is noticed. The authors explanation for this is that total radiation heat to the droplet is reducing with a factor proportional to d^2. And when droplet radius is very small radiation to droplet gets is very small and practically there is no external source of heat to supply the latent heat of vaporization and droplet uses its own thermal heat to vaporize and hence droplet cooles down very slowly. In models neglecting radiation heat, and only considering convection to the droplets, temperature stays steady after reaching to a maximum. In fact as convection coefficient h is inversly proportional to the droplet diameter(D). Then total convective heat to the surface of the droplet would be proportional to D. But total radiation to the droplet is proportional to D^2, and effect of droplet diameter is more significant in models including radiation heat.

Fig. 3 shows aseries of curves for radiation flux to droplets at the centerline of cylindrical chambers. The wall radiation becomes important in many cases. For example in the cylinders of 30cm radius with 30cm hot zone and 300cm radius with 150cm hot zone thickness, the wall radiation contributes 65% and 45% of the total radiation respectively. This happens when the wall temperature is taken to be the same as hot zone temperature(2000 °C). It is interesting to point out that the variation of the radiative flux in space upstream of the flame, is not drastic. As a first approximation constant radiation flux can be considered in some engineering calculations.

ACKNOWLEDGEMENT

The first author was supported financially by U.S. Army Research Office during the period of this study.

AIAA'83

AIAA-83-0152

A Study of Inter-phase Exchange Laws in Spray Combustion Modeling

S.K. Aggarwal, A.Y. Tong and W.A. Sirignano, Carnegie-Mellon Univ., Pittsburgh, PA

AIAA 21st Aerospace Sciences Meeting

January 10-13, 1983/Reno, Nevada

A STUDY OF INTER-PHASE EXCHANGE LAWS IN SPRAY COMBUSTION MODELING

S.K. Aggarwal*, A.Y. Tong**, W.A. Sirignano***[1]

Department of Mechanical Engineering
Carnegie-Mellon University
Pittsburgh, PA 15213

Abstract

The effects of different gas and liquid phase models on the vaporization behavior of a single component isolated droplet are studied for both the stagnant and the convection situations. In conjunction with four different liquid phase models, namely d^2-law, infinite conductivity, diffusion limit and internal vortex circulation, the different gas-phase models include a spherically symmetric model in the stagnant case and Ranz-Marshall correlation plus two other axisymmetric models in the convective case. A critical comparison of all of these models is made. The use of these models in a spray situation is also examined. A transient one-dimensional flow of an air-fuel droplet mixture is considered. It is shown that the fuel vapor mass fraction can be very sensitive to the particular liquid-phase and gas-phase models.

Nomenclature

C_p' = specific heat at constant pressure, cal/gm/°K

D' = $D\ D_c'$, gas diffusivity, cm^2/sec

H' = $H\ C_p'\ T_c'$, heat from the gas-phase given to the liquid phase per unit mass of fuel vaporized, cal/gm

L_c = length of the tube, cm

L' = $L\ C_p'\ T_c'$, heat of vaporization, cal/gm

L_r = L_c/r_o', ratio of gas-phase characteristic length and the initial drop size

M_f' = $M_f\ M_c'$, molecular weight of fuel

M_o' = $M_o\ M_c'$, molecular weight of oxidizer

m_k' = $m_k\ \rho_c'\ r_o'$, vaporization rate, gm/sec

n_k' = n_k/L_c^2, number of droplets per unit cross section area, $1/cm^2$

p' = $p\ p_c'$, gas pressure, atmosphere

r_k' = $r_k\ r_o'$, droplet radius, cm

T_c' = gas temperature at the tube entrance, °K

T' = $T\ T_c'$, gas temperature

T_k' = $T_k\ T_c'$, droplet surface temperature

t' = $t\ t_c'$, time

t_r = $t_c/D_c'/L_c^2$, ratio of convection time to diffusion time in the gas-phase

V_c' = gas velocity at the tube entrance, cm/sec

V' = $V\ V_c'$, gas velocity, cm/sec

V_k' = $V_k\ V_c'$, droplet velocity

x' = $x\ L_c'$, axial coordinate, cm

X_k' = $X_k\ L_c'$, droplet location

Y_{fs} = fuel vapor mass fraction at the droplet surface

Y_f = fuel vapor mass fraction

Y_o = oxidizer mass fraction

Y_N = neutral species mass fraction

Δx = spatial grid size

γ = ratio of specific heats

μ' = $\mu\ \mu_c'$, gas viscosity, gm/cm/sec

ϕ' = $\phi\ \phi_c'$, variable defined in Eq. (11)

ρ' = $\rho\ \rho_c'$, gas density

ρ_k' = liquid fuel density

ρ_r = ρ_c'/ρ_k', ratio of initial gas-phase density and the liquid fuel density

1. Introduction

Spray vaporization and combustion studies are of primary importance in predicting and improving the performance of systems utilizing spray injection. Combustors, fire suppression, spray drying and various forms of chemical power plants are typical examples of these systems. Often, the vaporization of a droplet in the spray is affected by neighboring droplets. However, in spray combustion computations, it is assumed that the overall spray behavior can be

[1] *Research Engineer and Lecturer, Member AIAA, **Graduate Student, ***G.T. Ladd Professor and Head, Member AIAA

obtained by summing behavior of individual isolated droplets surrounded by a gas-phase that itself has varying properties. Even when the assumption that droplets behave as if they were isolated from each other is not satisfactory, the behavior of a single isolated droplet in an oxidizing environment will still provide a fundamental input to the overall spray analysis.

A complete kinematic and vaporization study of an isolated droplet in a convective field involves the simultaneous description of the transport processes in both the gas and the liquid phases, the coupling between the phases, the phase change processes at the interface, and the chemical reaction in the gas-phase. However such a detailed model is too complex to be used in the spray computations at this time. As a result, several simplifying assumptions are made in the spray analysis. For example, it is assumed that the gas-phase processes around the droplet are quasi-steady, and that a phase equilibrium exists at the interface with the phase change being given by a Clausius-Clapeyron type relation. Also the assumptions of constant gas-phase transport properties and of a spherically symmetric flow field with a convective correction are often employed. In addition, the liquid phase transport processes may be completely neglected by using a d^2-law (constant droplet temperature) model [1] or by using an infinite conductivity (spatially uniform liquid temperature in the droplet) model [2]. The models based on the above assumptions are somewhat useful in that they simplify the problem considerably and thus provide easier solution to the problem. However there is a need to upgrade the droplet models in the spray analysis so that a better physical representation is given to transient behavior, liquid phase heat and mass transport, internal circulation, and gas-phase boundary layers. At the same time, there is a need to simplify the more complex droplet models so as to enhance their usefulness for the spray analysis. The work in this paper was undertaken to fulfill the above premise.

The basic droplet vaporization/combustion model for an isolated single component droplet in a stagnant environment was given by Godsave [1]. Since then this model has been extensively studied both experimentally and theoretically. These studies have been reviewed by Williams [4], Faeth [5] and Law [6]. More sophisticated studies have also been reported. These consider the effects of relaxing the restrictions of the basic model. Law and Law [7] considered the variable gas-phase transport property effects. Hubbard et al [8] considered the transient effects for the spherically - symmetric case and concluded that the quasi-steady gas-phase approximation yields small errors, at least for pressures below ten atmospheres. Their comparison with the constant transport property models using reference conditions indicated that the 1/3 rule gives the best agreement. There have also been studies on the transient droplet heating. These include the infinite liquid phase conductivity model [2] and conduction limit model [9]. It should be noted that the infinite conductivity model is an artificial one for the spherically symmetric case since no internal mechanism is present to increase the liquid heating rate above that of the conduction limit.

In many practical situations, the droplet vaporizes in a convective gas field. The gas-phase convection influences the vaporization process in two ways. First it increases the gasification rate as well as the heat transfer rate between the phases. Secondly it generates liquid circulation inside the droplet which increases the liquid heat transfer rate. Note that at very high relative velocity, droplet deformation and shattering can occur. This situation is not considered in this paper. Semi-empirical correlations [10] account for the gas-phase convection by expressing the vaporization and interphase heat transfer rates as a modification of the spherically symmetric case. Sirignano [11] analyzed the convective case through a combination of stagnation point and flat plate analyses and concluded that the convective case should not be treated by a correction on the spherically symmetric case. Prakash and Sirignano [12] analyzed the gas-phase and the liquid-phase flow fields for a single droplet in a convective gas field. They considered a gas phase boundary layer outside the droplet and a Hill's vortex in the droplet core with thin viscous and thermal boundary layers near the droplet surface and an inviscid internal wake near the axis of symmetry. Their results show that the infinite conductivity case is never realized and the characteristic liquid phase heat diffusion time reduces (from the diffusion-limit case) by an order of magnitude. Their analysis, however, is too complicated and computer-time consuming to be included in spray calculations. Tong and Sirignano [13] simplified this analysis substantially by neglecting the thin boundary layer inside the droplet surface. The results of this simplified model are in close agreement with those obtained from the more exact analysis [12]. The simplified vortex model and the other liquid phase heating models for a single droplet and for a spray situation are critically examined in the following sections. In Section 2, the effects of d^2-law, infinite conductivity, conduction limit, and vortex models on the vaporization behavior of a single component droplet are studied. Both the stagnant and the convective environments are considered. For the convective case, Ranz-Marshall correlation [10], an optimum average of the stagnation point region and the flat plate (droplet shoulder) region, and a more exact axisymmetric model are studied. All these gas-phase and liquid phase models are examined for three hydrocarbon fuels, namely, n-hexane, n-decane, and n-hexadecane. The use of different liquid phase models in a spray vaporization situation is described in Section 3, where a transient one-dimensional flow of an air-fuel droplet mixture in an open tube is considered. The effects of different droplet models on the fuel vapor mass fraction distribution in the tube are discussed in detail. An unsteadiness in the gas-phase properties, which is entirely due to the discrete droplet group locations, is also discussed. Conclusions are stated in Section 4.

2. Single Droplet Vaporization

Basically, the existing literature on single droplet vaporization can be classified into two major categories: spherically symmetric and axisymmetric. The different models in these two categories are discussed below.

2.1 Spherically Symmetric Models

2.1.1 d^2 Law Model. The most notable earlier work on droplet vaporization is by Godsave [1]. In that study, a quasi-steady spherically-symmetric model was used. The droplet temperature was assumed to be uniform and remained constant at its wet bulb value. The properties in both the gas and liquid phases were assumed to be constant, together with Lewis number equal to unity. At the gas-liquid interface, it was assumed that the fuel vapor mass fraction was a

function of the surface temperature given by some equilibrium vapor pressure equation such as the Clausius-Clapeyron relation. This theory gives the classic d^2-law and is the simplest possible model describing droplet vaporization. It should be noted that this model neglects the liquid phase heat and mass transfer and is basically a gas-phase model. It does not consider some of the important physics and only yields a crude estimate of the droplet vaporization rate.

Some of the resulting relationships are given below:

$$\frac{m}{4\pi r \rho_g D} = \ell n(1+B) \tag{1}$$

$$B = \frac{C_{pg}(T_g - T_s)}{L} = \frac{Y_{F_s}}{1 - Y_{F_s}} \tag{2}$$

where m is the fuel mass vaporization rate, B is the Spalding Transfer number, L is the latent heat of fuel and Y_{F_s} is the fuel vapor mass fraction at the interface. Subscripts g and s denote gas-phase and droplet surface, respectively.

Note that $Y_{F_s} = Y_{F_s}(T_s)$ is a function of surface temperature only. Therefore T_s and B can be determined by equation (2) and subsequently can be obtained through equation (1). For a given ambient condition, T_s and B are fixed in this model, equation (1) can be written as

$$\frac{dr^2}{dt} = k = \text{constant} \tag{3}$$

which says that the radius squared (proportional to the droplet surface area) decreases linearly in time and hence this model is referred to as d^2-law model in the literature.

2.1.2 Infinite Conductivity Model. In a combustor, the droplet is initially cold and heats up with time. The initial transient droplet heating period has only recently been given attention. Law [2] studied droplet combustion with rapid internal mixing where droplet temperature is spatially uniform but varying with time. It was found that droplet heating is a significant cause of the unsteadiness of droplet combustion and should be taken into account in any realistic analysis of unsteady droplet combustion phenomena. Basically, this model is the same as the d^2-law model except that the constant liquid phase temperature assumption is relaxed and is replaced by a uniform but time-varying temperature inside the droplet. The gas-phase model remains spherically symmetric and quasi-steady.

Some authors believed that this uniform temperature limit is related to the rapid internal liquid circulation limit and hence is referred to as rapid mixing model. Sirignano [11] showed that even in the limit of high vortex strength, the internal liquid circulation can only reduce the characteristic length scale for diffusion by an order of magnitude. The rapid mixing limit can never exist. Rather, it would be conceptually more correct to think that the uniform temperature limit results from the infinite conductivity limit. Hence it is more appropriate to call it an infinite-conductivity model.

Equations (1) and (2) remain the same except that L is replaced by

$$L + \frac{1}{m}\left(\frac{4}{3}\pi r^3 \rho_\ell c_{p\ell}\right)\frac{dT_\ell}{dt}.$$

The additional term accounts for the transient liquid droplet heating. Subscript ℓ denotes the liquid phase.

2.1.3 Conduction Limit Model. When the internal liquid motion is not significant, heat transfer inside the droplet will be controlled by thermal diffusion only. This will be a reasonable model for the stagnant case and represents the slowest heat transfer limit.

The liquid phase temperature variation is governed by the well known heat diffusion equation,

$$\frac{\partial T_\ell}{\partial t} = \frac{\alpha_\ell}{r^2}\frac{\partial}{\partial r}\left(r^2 \frac{\partial T}{\partial r}\right) \tag{4}$$

with the initial and boundary conditions

$$\begin{aligned} &\text{(i)} \quad \text{at } t = 0;\ T(r,\ t) = T_o(r) \\ &\text{(ii)} \quad \text{at } r = 0;\ \frac{\partial T(r,t)}{\partial r} = 0 \\ &\text{(iii)} \quad \text{at } r = r_s(t);\ k_\ell \frac{\partial T(r,t)}{\partial r} = q_\ell(t) \end{aligned} \tag{5}$$

where $T_o(r)$ is the initial temperature distribution and $q_\ell(t)$ is the liquid phase heat flux at the droplet surface.

Equations (1) and (2) remain essentially the same except that L is replaced by

$$L + \frac{1}{m}\left(4\pi r^2 k_\ell \frac{\partial T}{\partial r}\Big|_{r_s}\right).$$

The additional term accounts for the liquid phase heat flux at the surface.

Since the droplet is vaporizing, the diffusion field has a moving boundary. Obviously this model is more complicated than the infinite conductivity limit model.

2.2 Droplet Vaporization with Convective Effects

2.2.1 Ranz-Marshall Model. The studies discussed so far are based on the model of spherical symmetry. In reality, the practical problem of droplet vaporization in a spray involves a convective situation in which there is a relative gas-droplet velocity. Many investigators [4,5] suggested empirical correlations for vaporization rate in a convective field as a correction to the spherical symmetric case. The typical form of correlation is $m_{convection} = m_{spherical}\, f(Re,\ Pr)$ where f(Re, Pr) is the correction factor. In the present study, the Ranz-Marshall correlation is examined, for which the factor f(Re, Pr) is given by

$$f(Re,\ Pr) = 1 + 0.3\, Re^{1/2}\, Pr^{1/3} \tag{6}$$

Although this type of correlations is very simple, there is really very little theoretical justification for

them. Moreover, these correlations are based on experiments conducted under quasi-steady conditions. As mentioned before, there is a transient droplet heating stage and during that period the quasi-steadiness assumption is invalid. Indeed Sirignano [11] showed, through theoretical analysis, that a correlation of Ranz-Marshall type cannot satisfactorily predict the vaporization rate.

2.2.2 Prakash and Sirignano's Axisymmetric Model. Recently, Prakash and Sirignano [12, 14], studied the problem of transient liquid droplet vaporization in a hot convective environment. They first [14] studied liquid internal circulation and droplet heating and later [12] developed a gas-phase boundary layer analysis and coupled it to the previous liquid phase analysis. Basically, they used a two-dimensional axisymmetric model and divided the problem into several physical regions as shown in Figure 1. These regions were: outer inviscid gas flow, gas-phase boundary layer, liquid phase boundary layer, internal liquid wake and inviscid liquid core. Because of the relatively high Reynolds number and high Peclet number, the boundary layer approximation was used in their analysis for both the momentum and the energy transfers in both the gas and the liquid phases. The outer inviscid gas flow was treated as steady potential flow around a sphere with no flow separation.

The gas-phase and liquid-phase boundary layers were both treated as quasi-steady for both momentum and energy transfer, while for the liquid core, the momentum transfer was treated as quasi-steady and the energy transfer was considered transient. This model, named as Prakash and Sirignano's model here, has been included in the single droplet study. It should be mentioned that this model although quite detailed, uses an algorithm that is too cumbersome to be included in a complete combustion analysis. Simplifications, taking into account the important physics, are needed.

In Prakash and Sirignano's analysis, there is a thin thermal boundary layer near the droplet surface which is coupled to the thermal core in the matching region. The thermal boundary layer which allows for the heat flux to adjust from two-dimensional behavior along the droplet surface to one-dimensional behavior along the boundary layer and thermal core matching region, was treated as quasi-steady. The importance of the thermal boundary layer and the quasi-steadiness assumption have recently been reviewed by Tong and Sirignano [13]. The results of that study show that, unless the thermal boundary layer is very thin (very large Peclet numbers), the thermal inertia term is important and quasi-steadiness assumption for that layer is invalid. The results also tend to suggest that the elimination of the thermal boundary layer representation and the assumption that the thermal core solution is valid up to the droplet surface may still give solutions with acceptable degree of accuracy. It should be noted that while the thermal boundary layer formulation is two dimensional, the thermal core formulation is one-dimensional. Hence, the removal of the thermal boundary layer will simplify the problem tremendously. With the elimination of the thermal boundary layer and the assumption that the thermal core solution being valid up to the droplet surface, Tong and Sirignano [13] subsequently simplified the thermal core solution. Their simplified liquid phase model is included in this study.

2.2.3 Tong and Sirignano's Axisymmetric Model. Tong and Sirignano [15] further developed a one dimensional gas-phase model. They simplified the axisymmetric convective analysis in the gas-phase by representing the heat and mass transfer rates by an optimum average for the stagnation point region and the shoulder region of a droplet. The results from coupling this simplified gas model to their simplified liquid phase model which was obtained earlier are in reasonably good agreement with the results of the more detailed model of Prakash and Sirignano. This gas-phase model has been employed in the spray calculations to be reported in Section 3.

2.3 Results and Discussions

Liquid fuel droplets initially at 300 K vaporizing in 1000 K, 10 atm pressure fuel-free environment is used to study the various gas-phase and liquid-phase models. Hexane, decane and hexadecane droplets of initial radius of 0.00476 cm are considered. The physical properties are the same as those in the Prakash and Sirignano's analysis [12].

The results for the stagnant case are given in Figures 2 and 3. The gas-phase model is quasi-steady and spherically symmetric. Three different liquid phase models namely the d^2-law, the conduction limit and the infinite conductivity limit are compared. Since the existence of a vortex in a stagnant environment cannot be realized conceptually, it is excluded for comparison. One would think that if the vortex model were included, it would be in between the infinite conductivity limit and the conduction limit. This indeed can be shown to be true. Figures 2 and 3 show the temporal variation in the surface temperature and surface area respectively. The physical time, t is nondimensionalized by using the liquid thermal diffusivity, α_ℓ, and the initial droplet radius, r_o, as $\tau = t/(r_o^2/\alpha_\ell)$. For the d^2-law model the surface temperature is at the wet-bulb temperature and remains constant while the surface area regresses linearly in time. The d^2-law serves as an asymptotic limit for the other two models. This is reflected in Figure 2 where the surface temperature of the other two models approaches the wet bulb temperature and Figure 3 where the curves become more linear.

Since the d^2-law neglects the initial transient droplet heating, the droplet vaporizes much faster than the other two models. The difference is bigger for the heavier fuels which have higher boiling temperatures and hence longer transient heating period. Conversely, the conduction limit and the infinite conductivity limit have about the same droplet lifetime. Note that these two limits intersect each other. Since the droplet temperature is uniform in the infinite conductivity limit, the surface temperature increase per unit of energy absorption is less. Consequently, the fuel vapor mass fraction at the droplet surface is lower, which leads to lower vaporization rate. On the other hand, the difference between the ambient temperature and the surface temperature, which relates directly to the heat transfer rate to the liquid, is higher. This results eventually in a higher surface temperature and faster vaporization rate during the latter portion of the lifetime for the infinite conductivity model. Note that the wet-bulb temperatures in these calculations are considerably lower than their corresponding boiling temperatures of the fuels. The effect of the different liquid-phase models on the interior liquid temperature is quite significant and therefore the conduction limit model, which is considered to be exact, should be used. If detailed temperature distribution inside the droplet is

needed. The infinite conductivity model may be useful in the low ambient temperature case when the droplet lifetime is long. The d^2-law model which gives poor agreement with the conduction limit model is oversimplified and should be discarded.

The results for the convective case are given in Figures 4 to 7. In these calculations, the Reynolds number (based on droplet radius) is initially 100 and decreases with the radius as the droplet vaporizes. The relative velocity is 2500 cm/sec and is assumed to be constant throughout. In reality the relative velocity will be reduced by the drag force; this is considered later in the spray vaporization case.

Although Prakash and Sirignano's model is the most detailed and should be considered to be the most exact, it is quite cumbersome to be included in a complete spray analysis. Instead, Tong and Sirignano's model and the simplified vortex model which has been shown [15] to give close agreement with Prakash and Sirignano's results are used as reference model in the figures.

Figures 4 and 5 show the results of the various liquid phase models. The d^2-law does not exist in this convective case. Again, the conduction limit and the infinite conductivity limit intersect due to the same reasoning as that in the stagnant case. The vortex model lies in between the other two models as expected. Note that the droplet lifetime is considerably shorter than that in the stagnant case. In the convective case, $(r/r_o)^{3/2}$ regresses asymptotically linearly with time and it is used in Figures 5 and 7. Figure 5 shows that for the heavier fuel the percentage variation in droplet lifetime can depend quite significantly on the liquid phase model.

Figures 6 and 7 show the effects of the different gas-phase models. The Ranz-Marshall correlation overpredicts the vaporization rate and underestimates (for decane) the surface temperature. As indicated by Sirignano [11], this type of correlation has very little theoretical justification and cannot give satisfactory results. The present study supports Sirignano's qualitative analysis. Tong and Sirignano's model appear to be in good agreement with the more detailed model of Prakash and Sirignano.

The results indicate that the droplet heating and vaporization are essentially unsteady for most of its lifetime, particularly for the heavier fuel. For a detailed analysis, Prakash and Sirignano's model is recommended but for more practical application, Tong and Sirignano's model with the simplified vortex model would be useful.

3. SPRAY VAPORIZATION STUDY

In the spray vaporization problem, a one-dimensional transient flow of air and fuel droplets in an open tube is considered, where the motion and vaporization of a monodispersed spray in a laminar, hot gas stream are studied. The purpose is to examine the effects of different liquid phase models on the bulk vaporization characteristics as well as on the gas medium. The different liquid-phase models considered are the infinite conductivity, the conduction limit, and the vortex models. The different convective models for the gas-phase are the Ranz-Marshall correlation and the model of Tong and Sirignano. The physical situation consists of a continuous laminar flow of hot air in an open tube. The gas-phase properties initially in the tube and later at the tube entrance are prescribed. The injection of fuel droplets is intermittent. One group of droplets is injected every given time interval. The number of droplets in a group (or with a characteristic) represents the number of droplets per unit cross-section area. The frequency of injection and initial droplet velocity depends on the overall fuel-air ratio in the tube, the mass flow of air, droplet spacing and droplet diameter at the tube entrance. The prescription of the overall fuel-air ratio, the droplet diameter and the droplet velocity at the entrance yields the value of the droplet number density. The droplet spacing in the axial direction and the number of droplets per unit cross-section area are so adjusted as to provide initially an isotropic droplet spacing in a unit cube. Initially a high relative velocity is provided between the two phases. As a droplet group moves in the hot gas stream, it accelerates. At the same time, the droplets heating and vaporization is taking place. The spray processes influence the state of the gas, i.e., the gas-phase is continuously retarded, cooled, and enriched with fuel vapor. The gas-phase properties are also being influenced by the upstream convection. All these gas-phase and liquid-phase processes are modeled by a system of unsteady, one-dimensional equations. The gas-phase is represented in Eulerian coordinates whereas the liquid phase is represented in Lagrangian coordinates. The governing equations in the non-dimensional form are given as follows:

GAS PHASE EQUATIONS

$$\frac{\partial \rho}{\partial t} + \frac{\partial}{\partial x}(\rho V) = S_\rho \tag{7}$$

$$\frac{\partial Y}{\partial t} + V\frac{\partial Y}{\partial x} - t_r D\frac{\partial^2 Y}{\partial x^2} = S_Y \tag{8}$$

$$Y = Y_f,\ Y_o,\ \phi \tag{9}$$

$$Y_N = 1.0 - Y_f - Y_o \tag{10}$$

$$\phi = T\,p\,\frac{1-\gamma}{\gamma} \tag{11}$$

$$\rho = \frac{p^{1/\gamma}}{\phi}$$

LIQUID-PHASE EQUATIONS

$$\frac{dX_k}{dt} = V_k \tag{13}$$

$$\frac{dV_k}{dt} = \left\{\rho_r L_r^2 t_r\right\}\left\{\frac{3}{16}\frac{C_D\,\mu\,Re_k\,(V-V_k)}{S_k}\right\} \tag{14}$$

$$\frac{dS_k}{dt} = -2\left\{\rho_r L_r^2 t_r\right\}(1 + 0.3\,Re_k^{0.5})\ln(1 + B_k)$$

for Ranz-Marshall correction model (15)

$$\frac{dS_k}{dt} = -2\left\{\rho_r L_r^2 t_r\right\}\left[\frac{2}{\pi} Re_k\right]^{0.5} f(B')$$

for Tong - Sirignano Model

$$S_k = r_k^2 \tag{16}$$

$$C_D = \frac{24}{Re_k}\left(1 + \frac{Re_k^{2/3}}{6}\right) \tag{17}$$

$$Re_k = \frac{2}{t_r L_r}\frac{r_k \rho}{\mu}\,|\,V - V_k\,| \tag{18}$$

$$\mu = \mu(T'_{ref}) = \frac{1}{\mu_o}\left[\frac{b\,T'^{3/2}_{ref}}{S + T'_{ref}}\right] \tag{19}$$

$$\text{where } T'_{ref} = \frac{1}{3}T' + \frac{2}{3}T'_k \tag{20}$$

The source terms in the gas-phase equations result from the coupling between the two phases. These are given in the Appendix. It should be noted that a transformation as given by Eq. (11) has been employed. This transformation is useful for a constant volume situation [16]. However, it has been retained here (a constant pressure case) for the sake of generality.

In non-dimensionalizing the gas-phase equations, the length scale is the length of the tube, and the velocity scale is the gas velocity at the tube entrance. The time scale is determined by these two scales. The gas-phase properties are non-dimensionalized by using the respective properties at the entrance. For the liquid phase equations, the droplet location, velocity and surface temperature are respectively non-dimensionalized by the gas-phase length, velocity and temperature scales. The droplet radius is non-dimensionalized by the initial droplet radius. The above non-dimensionalization gives rise to three additional dimensionless groups, t_r, L_r and ρ_r; t_r is the ratio of convective time to diffusion time in the gas-phase, L_r is the ratio of gas-phase length scale and initial drop radius, and ρ_r is the ratio of initial gas-phase density and liquid density.

The important assumptions made in writing these equations are that the gas pressure is constant, radiative heat transfer is negligible, the species diffusion follows Fick's law with equal mass diffusivities for each pair, the specific heat at constant pressure is constant, and the gas phase Lewis and Schmidt numbers are unity. In addition, the product $\rho D(=\mu)$ is assumed constant. It is noteworthy, however, that in the calculation of liquid-phase properties μ is considered a function of temperature as given by Sutherland correlation [17]. As indicated in Eq. (19), a reference temperature is used for the calculation of μ and the reference temperature is obtained by 1/3 rule as recommended by Sparrow and Gregg [18].

The drag coefficient is evaluated by using an expression as proposed by Putnam [19]. The evaluation of Reynold's number for the drag coefficient is based on the free stream density and viscosity evaluated at the 1/3 reference state. This follows the recommendation of Yuen and Chen [20]. It should also be noted that the effect of relative droplet-gas velocity on the vaporization rate [see Eq. (15)] has been treated by a semi-empirical correlation [10], as well as by an axisymmetric model [15].

3.1 The Solution Procedure

A hybrid Eulerian Lagrangian numerical scheme is used to calculate the gas-phase and liquid-phase properties at the $(n+1)^{th}$ time level from the values known at the n^{th} time level. First of all, a second-order accurate scheme is employed to interpolate the gas-phase properties from the Eulerian locations (fixed grid points) to the Lagrangian (or droplet) locations. The scheme uses the gas-phase properties at two grid points x_i and x_{i+1} and gives the corresponding properties at a Lagrangian location X_k, where X_k is between x_i and x_{i+1}. Using these gas-phase properties, the droplet surface temperature is then calculated. For the infinite conductivity model, it involves the solution of an ordinary differential equation for each droplet group. For the conduction limit and vortex models, a partial differential equation needs to be solved. The details have been discussed in Section 2. Knowing T_k for each droplet group, other droplet properties (X_k, V_k, r_k) can be obtained by solving Eqs. (13) - (16). A second-order Runge-Kutta scheme is used for this purpose. It should be noted, however, that there is some loss of accuracy due to the fact that the gas-phase properties are not updated in the Runge-Kutta scheme. Using the new liquid-phase properties, the source terms as given in the Appendix can be evaluated at the Lagrangian locations. Then a second-order accurate scheme is used to distribute these source terms from a Lagrangian location to the two neighboring gas-phase locations. Using these source terms, the gas-phase properties (Y_f, Y_o and ϕ) at the $(n+1)^{th}$ time level are obtained by solving Eq. (8). An explicit finite-difference method is used for this purpose. The gas temperature and gas density are then obtained by using Eqs. (11) and (12). Finally the gas velocity is obtained from an integral form of the continuity equation (7). It is worth emphasizing that in the present case, the gas-phase convection term dominates the diffusion term. Therefore, an upwind difference scheme [21] is employed for the convection term. It should also be noted that an explicit method was found to be the most efficient for reacting two-phase flow [21]. However, an implicit method may be more efficient for the present vaporizing case without combustion since the equations may not be as stiff.

3.2 Discussion of Results

The effects of using different liquid-phase models on the bulk spray and gas-phase properties are now discussed. The various values used in the computation are listed in Table 1. The criterion used in selecting these values was to consider a spray vaporization situation with a moderate gas-phase convection for the droplets. The selected values provide an initial Reynold's number (based on the relative velocity and the drop radius) of 56.5 and a droplet residence time of about 12.5 msec. During this time, eighty percent of

the droplet mass is vaporized. The effects of different liquid-phase models on the bulk gas-phase properties is presented in Figs. 8 - 11. Figures 8 and 9 indicate that the choice of a particular droplet heating model can significantly influence the fuel vapor distribution in the tube. This can have a profound effect on the subsequent combustion process in a practical situation. The maximum difference between the fuel vapor mass fraction values is as much as one hundred percent between the conduction limit and the infinite conductivity models. As Fig. 9 indicates, the conduction model initially (up to a distance of 5 cm) predicts the highest fuel vapor mass fraction, whereas the infinite conductivity model predicts the lowest. At later times the situation is reversed. The vortex model results are always in between those of the other two models. The difference in the fuel vapor distribution is a direct consequence of the difference in the droplet surface temperature values for the three models. As discussed in Section 2, the conduction limit model initially predicts the highest droplet surface temperature and therefore the fastest vaporization rate, whereas the infinite conductivity model predicts the lowest surface temperature and the slowest vaporization rate. As also discussed in Section 2, this behavior is reversed at later times.

The fuel vapor mass fraction profiles in Figs. 8 and 9 exhibit an oscillatory behavior. This is due to the periodic nature of the droplet injection process which causes a finite droplet spacing in the streamwise direction. Thus the period of this oscillation is the same as the time interval between two subsequent injections. This is clearly illustrated in Fig. 10. As this figure indicates the profiles overlap after every 0.5 msec, which is the time interval between two subsequent injections. This unsteady gas-phase behavior, which is entirely due to the spray discretization, should be kept in mind in spray modeling. The gas temperature profiles at time = 16 msec for the three liquid models are shown in Fig. 11. The continuous drop in the gas temperature is indicative of the continuous cooling of the gas-phase due to droplet heating and vaporization. The difference in the gas temperature distribution due to the different liquid phase models is not as significant as that in the fuel vapor distribution. This is due to the fact that the spray heating and vaporization constitute only a small heat loss in the overall gas-phase heat budget. The oscillatory behavior in the gas temperature profiles is again due to the intermittent droplet injection process. This intermittency is prescribed exactly in our idealized calculation. In a practical situation, it may not be so well-defined and perhaps should be taken as random. That is, the distance between droplets as they flow into the domain of interest will not be fixed as they are given in this calculation but rather will be distributed about some average value.

The effect of different liquid heating models on the droplet properties is illustrated in Table 2. The properties of the first droplet group, i.e. the location, the non-dimensional radius, the surface temperature, and the velocity are given as functions of time for the three models. The difference in the surface temperature and droplet radius values for the three models is very similar to that discussed in Section 2. The conduction limit model predicts the highest droplet velocity, whereas the infinite conductivity model predicts the lowest value. This occurs since the conduction limit model initially predicts the fastest vaporization rate, the smallest drop size, and consequently the highest droplet acceleration. It should be noted, however, that the difference in the droplet velocities for the three models is quite small.

The effect of different convective models is presented in Figs. 12 - 13. It should be noted that the model of Tong and Sirignano is valid only when the Reynolds number is significant; as indicated by Eq. (15), this model predicts a vaporization rate, which is proportional to the square root of the Reynolds number. For this reason, initial droplet radius of 100 microns is used for these calculations. This gives a value of 112 for the initial Reynolds number. Figure 12 shows that the Ranz-Marshall correlation overpredicts the vaporization rate as compared to that given by the axisymmetric model. This behavior is consistent with the one observed for the single droplet case in the previous section. Figure 13 gives the differences in the gas temperature distribution for the two models. Since the Ranz-Marshall correlation model predicts a higher vaporization rate and therefore a higher heat loss from the gas phase, it gives lower gas temperatures than those given by the other model. It is also important to note that at very small Reynolds number, the axisymmetric model predicts an unacceptably small vaporization rate. Consequently a more realistic spray model should have the capability to switch from the axisymmetric model to a Ranz-Marshall correlation type of model as the Reynolds number becomes small. This is presently under investigation.

4. Conclusions

The most common vaporization models have been compared for fuels of varying volatibility and droplets in a high-temperature environment. Both isolated droplet and spray vaporization have been studied. The use of the d^2-law or the infinite-conductivity model (sometimes named the rapid mixing model) has been shown to be very inadequate. For spherically-symmetric vaporization (no relative gas-droplet motion), the conduction limit model for transient heating is recommended. In practical situations where a relative gas-droplet motion exists, the simplified vortex model of Tong and Sirignano is recommended when the Reynolds number based on relative velocity is high. That model compares well with the more detailed model of Prakash and Sirignano and predicts well the effects of the laminar gas-phase boundary layer over the droplet and the internal circulation in the droplet.

The spray calculations indicate an inherent unsteadiness due to the intermittent character of a spray. This unsteadiness will be interesting whenever we wish to resolve structure on the scale of the average distance between droplets.

References

1. Godsave, G.A.E., "Studies of the Combustion of Drops in a Fuel Spray: The Burning of Single Drops of Fuel," *Symposium (International) on Combustion*," Williams and Wilkins, Baltimore, 1953, pp. 818-830.

2. Law, C.K., "Unsteady Droplet Vaporization with Droplet Heating," *Combustion and Flame*, Vol. 26, 1976, pp. 17-22.

3. Spalding, D.B., "The Combustion of Liquid Fuels," *Fourth Symposium (International) on Combustion*, Williams and Wilkins, Baltimore, 1953, pp. 847-864.

4. Williams, A., "Combustion of Droplets of Liquid Fuels: A Review," *Combustion and Flame*, Vol. 21, 1973, pp. 1-31.

5. Faeth, G.M., "Current Status of Droplet and Liquid Combustion," *Proc. Energy Combustion Sci.*, Vol. 3, 1977, pp. 191-224.

6. Law, C.K., "Recent Advances in Droplet Vaporization and Combustion," *Proc. Energy Combustion Sci.*, Vol. 8, 1982, pp. 171-201.

7. Law, C.K. and Law, H.K., "Theory of Quasi-Steady One-Dimensional Diffusional Combustion with Variable Properties Including Distinct Binary Diffusion-Coefficients," *Combustion and Flame*, Vol. 29, 1977, pp. 269-275.

8. Hubbard, G.L., Danny, V.E., and Mills, A.F., "Droplet Vaporization: Effects of Transients and Variable Properties," *Int. J. Heat Mass Transfer*, Vol. 18, 1975, pp. 1003-1008.

9. Law, C.K. and Sirignano, W.A., "Unsteady Droplet Combustion with Droplet Heating II, Conduction Limit," *Combustion and Flame*, Vol. 29, 1977, pp. 175-186.

10. Ranz, W.E. and Marshall, W.R., "Evaporation from Drops," *Chemical Engineering Progress*, Vol. 48, 1952, pp. 141-146, and 173-180.

11. Sirignano, W.A., "Theory of Multi-Component Fuel Droplet Vaporization," *Archives of Thermodynamics and Combustion*, Vol. 9, No. 2, 1978, pp. 231-247.

12. Prakash, S. and Sirignano, W.A., "Theory of Convective Droplet Vaporization With Unsteady Heat Transfer in the Circulating Liquid Phase," *Int. J. Heat Mass Transfer*, Vol. 23, No. 3, 1980, pp. 253-268.

13. Tong, A. and Sirignano, W.A., "Analytical Solution for Diffusion and Circulation in a Vaporizing Droplet," *19th (International) Symposium on Combustion*, Haifa, Israel, 1982.

14. Prakash, S. and Sirignano, W.A., "Liquid Fuel Droplet Heating with Internal Circulation," *Int. J. Heat Mass Transfer*, Vol. 21, 1978, pp. 885-895.

15. Tong, A.Y. and Sirignano, W.A., "Analysis of Vaporizing Droplet with Slip, Internal Circulation and Unsteady Liquid Phase Heat Transfer," Submitted to the *JSME-ASME Thermal Engineering Joint Conference*, Honolulu, Hawaii, (March, 1983).

16. Seth, B., Aggarwal, S.K., and Sirignano, W.A., "Flame Propagation Through an Air-Fuel Spray Mixture with Transient Droplet Vaporization," *Combustion and Flame*, Vol. 39, 1980, pp. 149-168.

17. Fox, R.W. and McDonald, A.T., "Introduction to Fluid Dynamics," *John Wiley and Sons*, 1978, pp. 613-616.

18. Sparrow, E.M. and Gregg, J.L., *Trans. ASME*, Vol. 80, 1958, pp. 879-886.

19. Putnam, A., *ARSJ.*, Vol. 31, 1961, pp. 1467-1468.

20. Yuen, M.C. and Chen, L.W., "On Drag of Evaporating Droplets," *Combustion Sci. Technology*, Vol. 14, 1976, pp. 147-154.

21. Aggarwal, S.K. and Sirignano, W.A., "Effect of Numerical Modeling on One-Dimensional Enclosed Homogeneous and Heterogeneous Deflagrations," *ASME Winter Annual Meeting*, Paper No. 81-WA/HT-46, 1981.

22. Sirignano, W.A., "Fuel Vaproization and Spray Combustion Theory," Submitted to the *Proc. Energy Combustion Sci.*

Appendix

The source/sink terms in the gas-phase equations (1, 2) are given as follows:

$$S_\rho = \frac{t_r}{L_r}\frac{1}{\Delta x}\sum_k \dot{m}_k n_k \tag{21}$$

$$S_{Y_f} = \frac{1}{\rho} S_\rho (1-Y_f) \tag{22}$$

$$S_{Y_o} = -\frac{1}{\rho} S_\rho Y_o \tag{23}$$

$$S_\phi = -\frac{S_\rho}{\rho}\frac{p}{\frac{\gamma-1}{\gamma}}\left\{H + T - T_k\right\} \tag{24}$$

$$\dot{m}_k = 4\pi r_k \mu (1 + 0.3\,Re_k^{0.5}) \ln(1 + B_k)$$
for Ranz-Marshall Correlation (25)

$$B_k = \frac{T-T_k}{H} \tag{26}$$

$$H = \frac{(1-Y_{fs})(T-T_k)}{Y_{fs} - Y_f} \tag{27}$$

$$Y_{fs}^{-1} = 1 + \frac{M_a'}{M_f'}(x_{fs}^{-1} - 1) \tag{28}$$

$$x_{fs} = \frac{p_n'}{p'} \exp\left[\frac{L' M_f'}{R'}\left(\frac{1}{T_{bn}'} - \frac{1}{T_k'}\right)\right] \tag{29}$$

In the above relations, S_{Yf} and S_{Yo} are the source and sink terms for the fuel vapor and oxidizer mass fractions, x_{fs} is the mole fraction at the droplet surface, M_s' is the molecular weight of the gas-phase (excluding fuel vapor), T_{bn}' is the liquid fuel boiling temperature at the normal pressure p_n', p is the prevailing pressure, and Σ represents the summation over all droplet groups which happen to be in a given gas-phase mesh, of size Δx. A phase equilibrium assumption has been made at the droplet surface and the Clausius-Clapeyron relation [Eq. 29] has been used. The different methods of computing the droplet surface temperature T_s distinguish the various liquid phase models examined in the present spray problem. These have been discussed in Section 2.

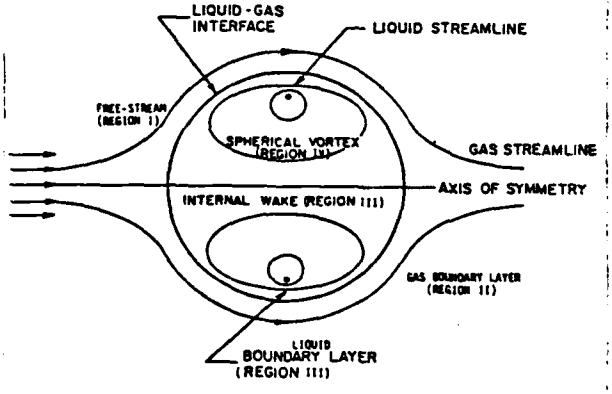

FIG. 1 FLOW REGIONS OUTSIDE AND WITHIN A FUEL DROPLET AT HIGH REYNOLDS NUMBER (From Ref. 22)

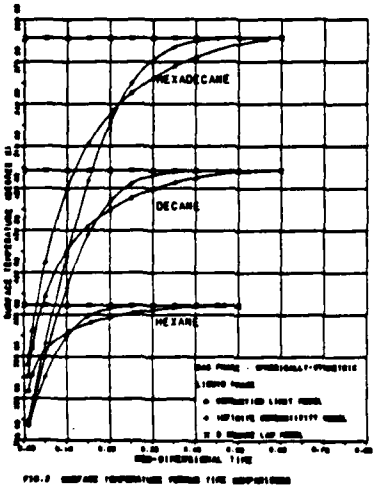

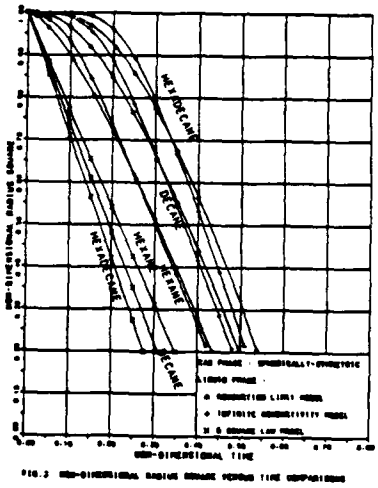

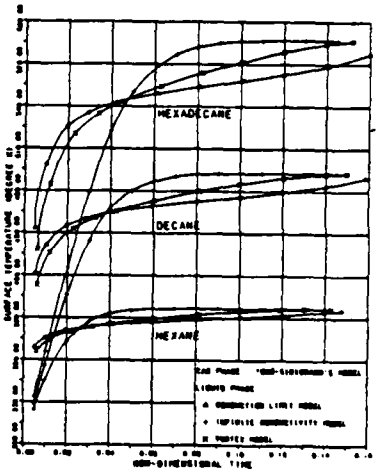

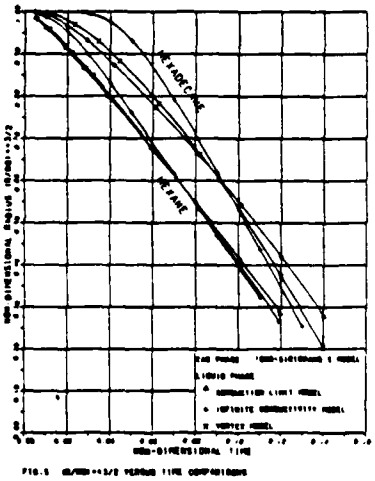

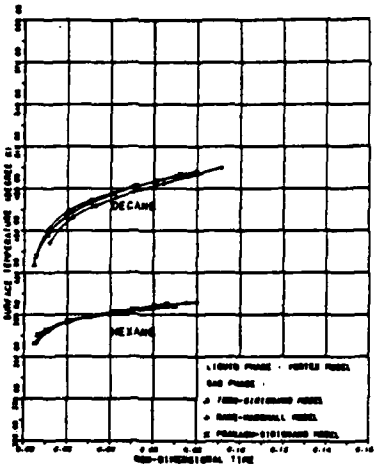

FIG.6

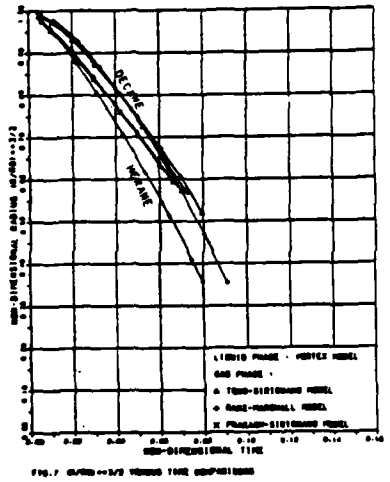

FIG.7

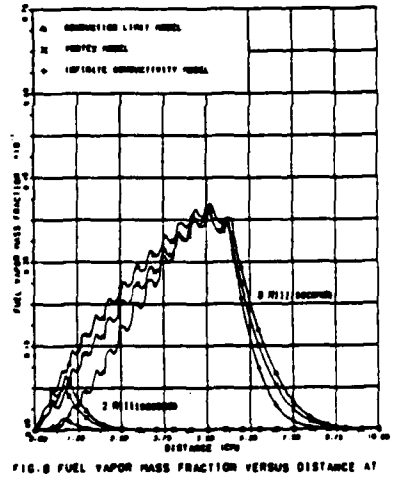

FIG.8 FUEL VAPOR MASS FRACTION VERSUS DISTANCE AT VARIOUS TIMES FOR DIFFERENT LIQUID-PHASE MODELS

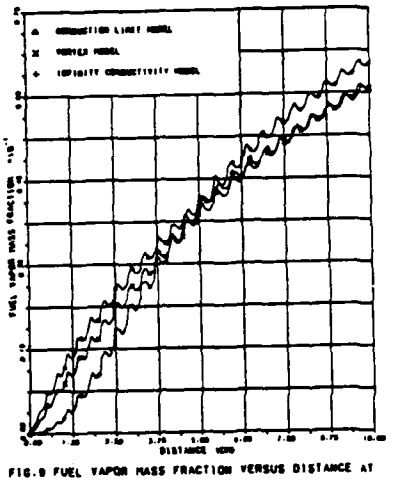

FIG.9 FUEL VAPOR MASS FRACTION VERSUS DISTANCE AT 16 MILLISECONDS FOR DIFFERENT LIQUID-PHASE MODELS

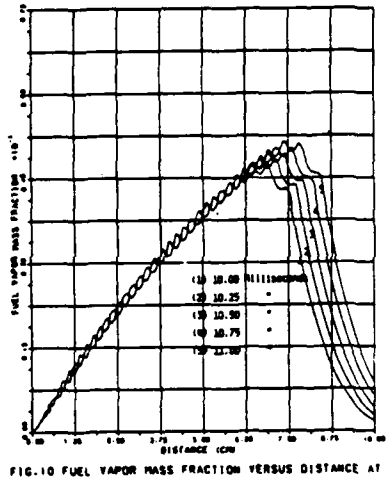

FIG.10 FUEL VAPOR MASS FRACTION VERSUS DISTANCE AT VARIOUS TIMES FOR THE VORTEX MODEL

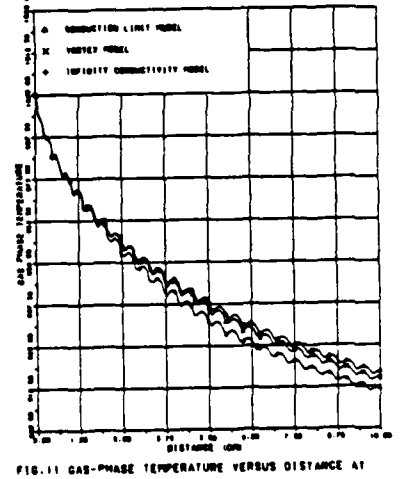

FIG.11 GAS-PHASE TEMPERATURE VERSUS DISTANCE AT 16 MILLISECONDS FOR DIFFERENT LIQUID-PHASE MODELS

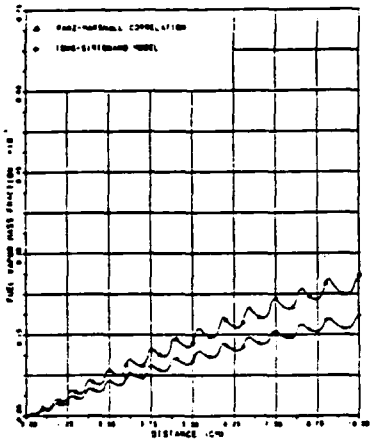

FIG. 12 FUEL VAPOR MASS FRACTION VERSUS DISTANCE AT 16 MILLISECONDS FOR DIFFERENT GAS-PHASE MODELS

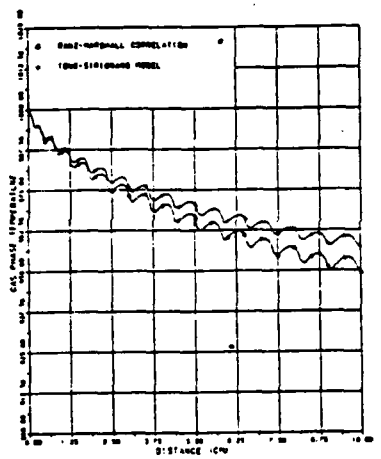

FIG. 13 GAS-PHASE TEMPERATURE VERSUS DISTANCE AT 16 MILLISECONDS FOR DIFFERENT LIQUID-PHASE MODELS

Table 1: Values of Various Parameters Used in Spray Calculations

Parameter	Value
Fuel	N-Decane
Liquid Density	$\rho'_\ell = 0.773$
Initial Drop Radius	$r'_0 = 50$ microns
Initial Drop Temperature	$T'_\ell = 300°K$
Number of Drops per unit cross-section area	$N'_\ell = 400$ 1/cm^2
Drop spacing in the axial direction	$d'_\ell = 0.05$ cm
Gas velocity at the tube entrance	$V'_c = 1000$ cm/sec
Drop Velocity at the tube entrance	$V'_\ell = 0.1\ V'_c$
Tube length	$L_c = 10$ cm
Pressure	$p'_c = 10$ atm
Gas temperature at the entrance	$T'_c = 1000°K$
Temporal step size	$\Delta t' = 10^{-5}$ sec
Spatial step size	$\Delta x' = 0.1$ cm
Specific heat at constant pressure	$C'_p = 0.25$ cal/gm°K
Molecular weight of fuel	$M'_f = 142.3$ gm/mole
Molecular weight of oxidizer	$M'_o = 32.0$
Boiling temperature of the Fuel at 1 atm	$T'_{BP} = 447.3°K$
Heat of vaporization	$L' = 86.5$ cal/gm
Gas constant	$R'_{GAS} = 2.8393$ atm cm^3/gm-°K

Table 2: Properties of the First Droplet Group for Different Liquid Phase Models

Conduction Limit Model

t(msec)	X_ℓ(cm)	r_ℓ/r_0	T_ℓ(°K)	V_ℓ(cm/sec)
0	0	1.0	300.0	100.0
2	0.885	0.981	445.0	590.0
4	2.272	0.902	453.3	773.1
6	3.916	0.842	458.1	861.2
8	5.691	0.781	462.2	909.2
10	7.540	0.716	465.9	937.2
12	9.433	0.648	469.1	954.5

Infinite Conductivity Model

t(msec)	X_ℓ(cm)	r_ℓ/r_0	T_ℓ(°K)	V_ℓ(cm/sec)
0	0	1.0	300.0	100.0
2	0.889	0.994	412.5	587.6
4	2.257	0.948	459.4	758.2
6	3.869	0.867	471.8	845.0
8	5.618	0.779	474.5	897.1
10	7.445	0.692	475.0	930.3
12	9.328	0.604	475.1	951.6

Vortex Model

t(msec)	X_ℓ(cm)	r_ℓ/r_0	T_ℓ(°K)	V_ℓ(cm/sec)
0	0	1.0	300.0	100.0
2	0.885	0.973	438.1	588.0
4	2.264	0.92	452.6	767.5
6	3.895	0.858	460.6	854.7
8	5.658	0.791	465.6	903.4
10	7.496	0.721	468.8	932.7
12	9.382	0.648	470.9	951.3

Submitted to Journal of Computational Phys.

Two-Phase Laminar Axisymmetric Jet Flow: Explicit, Implicit, and Split-Operator Approximations

S.K. Aggarwal, G.J. Fix, W.A. Sirignano

Carnegie-Mellon University

Pittsburgh, PA 15213

To appear in Computers and Fluids

NUMERICAL MODELING OF ONE-DIMENSIONAL ENCLOSED HOMOGENEOUS AND HETEROGENEOUS DEFLAGRATIONS

S. K. Aggarwal and W. A. Sirignano
Mechanical Engineering Department
Carnegie-Mellon University
Pittsburgh, Pennsylvania 15213

ABSTRACT

The objective of this study is to evaluate the effectiveness of several finite difference techniques in modeling unsteady homogeneous and heterogeneous flames in closed combustors. The problem of propagation of a pre-mixed homogeneous flame and a heterogeneous flame in air-fuel droplet-fuel vapor mixture is formulated. The governing equations have been solved using five different numerical techniques, an explicit method, an iterative implicit method without any formal linearization, an iterative implicit method with quasi-linearization, a non-iterative time-linearization block implicit scheme, and an operator-splitting method. The results are obtained in terms of the profiles of gas and liquid phase properties at different instances of time as the flame traverses the combustor. From these results, the relative efficiency and accuracy of each of the numerical techniques are discussed.

A HYBRID EULERIAN-LAGRANGIAN METHOD FOR ONE-DIMENSIONAL UNSTEADY SPRAY FLAMES

S. K. Aggarwal
Department of Mechanical Engineering
Carnegie-Mellon University
Pittsburgh, Pennsylvania 15213

July 1983

ABSTRACT

A hybrid Eulerian-Lagrangian method is employed to study a laminar unsteady propagating flame through an air/fuel-vapor/fuel-droplet mixture in a one-dimensional combustor. The gas-phase properties are obtained by using a continuum approach, whereas the computation of liquid-phase properties is based on a Lagrangian approach. A quiescent mixture of air and fuel mist is ignited by providing a hot wall at the end of the combustor. Following ignition, a flame initiates and propagates into the cold spray mixture. The characteristics of the propagating spray flame are presented in terms of the profiles of gas-phase and liquid-phase properties. Effects of droplet heating models, overall equivalence ratio, fuel volatility and initial droplet size are discussed. Results for the infinite-conductivity model and the conduction limit model, which represent the fastest and the slowest heat transport modes in the droplet interior respectively, indicate that the droplet heating models have only a minor effect on the bulk spray flame characteristics, when the overall mixture is close to stoichiometric. However, when the overall mixture is either fuel rich or fuel lean, the differences in heating models are significant. An increase in fuel volality and/or a reduction in initial drop size enhances the speed of flame propagation, and imparts a premixed type character to the flame.

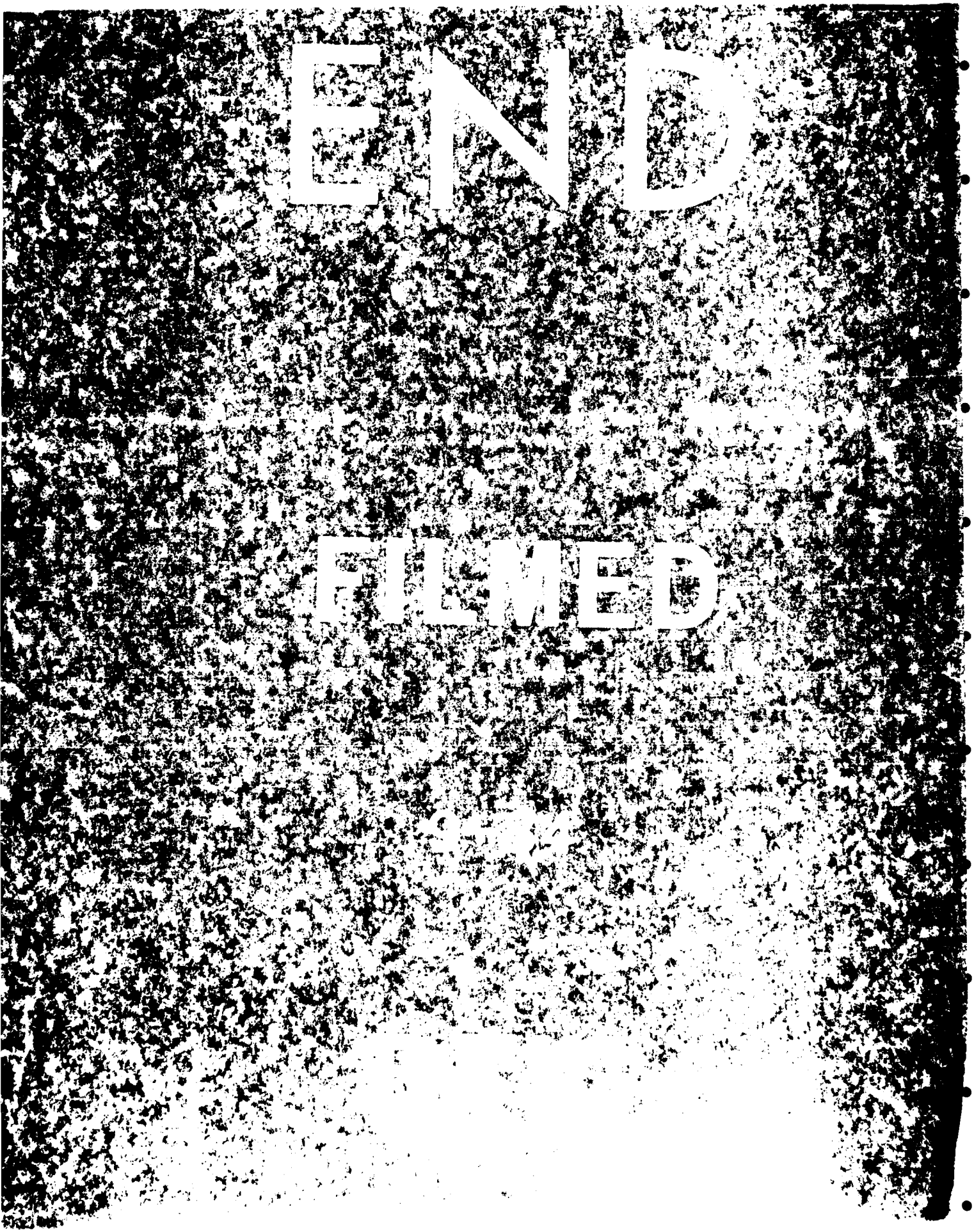
END
FILMED